Base-Salt Relief Controls on Salt-Tectonic Structural Style, São Paulo Plateau, Santos Basin, Brazil

*Leonardo M. Pichel[1], Christopher A-L. Jackson[1]; Frank Peel[1,2], Tim P. Dooley[2]

1 – Basins Research Group (BRG), Department of Earth Science and Engineering, Imperial College London, South Kensington Campus, SW7 2BP, United Kingdom

2 – The University of Texas at Austin, Bureau of Economic Geology, Jackson School of Geosciences, Austin, Texas, USA

Key-words: SALT TECTONICS, MINIBASINS, DIAPIRISM, TRANSLATION, BASE-SALT RELIEF, RAMP-SYNCLINE BASINS, GRAVITY-DRIVEN DEFORMATION, SANTOS BASIN, BRAZIL, SÃO PAULO PLATEAU

ABSTRACT

Base-salt relief influences salt flow, producing three-dimensionally complex strains and multiphase deformation within the salt and its overburden. Understanding how base-salt relief influences salt-related deformation is important to correctly interpret salt basin kinematics and distribution of structural domains, which have important implications to understand the development of key petroleum system elements. The São Paulo Plateau, Santos Basin, Brazil is characterized by a >2 km thick, mechanically layered Aptian salt layer deposited above prominent base-salt relief. We use 3D seismic reflection data, and physical and conceptual kinematic models to investigate how gravity-driven translation above thick salt, underlain by complex base-salt relief, generated a complex framework of salt structures and minibasins. We show that ramp-syncline basins developed above and downdip of the main pre-salt highs record c. 30 km of Late Cretaceous-Paleocene basinward translation. As salt and overburden translated downdip, salt flux variations caused by the base-salt relief resulted in non-uniform motion of the cover, and the simultaneous development of extensional and contractional structures. Contraction preferentially occurred where salt flow locally decelerated, above landward-dipping base-salt ramps and downdip of basinward-dipping ramps. Extension occurred at the top of basinward-dipping ramps and base-salt plateaus, where salt flow locally accelerated. Where the base of the salt layer was broadly flat, structures evolved primarily by load-driven passive diapirism. At the edge of or around smaller base-salt highs, salt structures were affected by plan-view rotation, shearing and divergent flow. The magnitude of translation (c. 30 km) and the style of salt-related deformation observed on the São Paulo Plateau afford an improved kinematic model for the enigmatic Albian Gap, suggesting this structure formed by a combination of basinward salt expulsion and

regional extension. These observations contribute to the long-lived debate regarding the mechanisms of salt tectonics on the São Paulo Plateau, ultimately improving our general understanding of the effects of base-salt relief on salt tectonics in other basins.

1. Introduction

Gravity-driven salt-related deformation along passive margins is typically characterised by an updip domain of extension and a downdip domain of kinematically-linked contraction, connected by a broadly undeformed zone of translation (Fig. 1a) (Rowan et al., 2000; 2004; Hudec and Jackson, 2004, 2007; Brun and Fort, 2011; Quirk et al., 2012; Jackson et al., 2015a). However, recent studies demonstrate this represents a simplified view of salt tectonics, with salt flow and related overburden translation across base-salt relief generating complex multiphase deformation and strains (Fig. 1b) (Dooley et al., 2016; Dooley and Hudec, 20162016; Pichel et al., 2018; 2019). The translational domain, previously thought of as a structurally simple region, can instead undergo a highly complex kinematic history and thus be intensely deformed. Explicitly recognising that base-salt relief can control salt flow and overburden translation can help improve margin-scale kinematic analyses of salt basins. For example, the translational domain may contain an explicit record of the magnitude and direction of net-basinward tectonic transport, aiding structural restorations (Jackson and Hudec, 2005; Pichel et al., 2018). Understanding margin-scale salt-tectonics is not only of academic interest, but can also aid ongoing hydrocarbon exploration along the margin. For example, it is critical to know the timing of salt-related deformation, hydrocarbon migration and trap formation relative to deposition of key petroleum systems elements (e.g. source, reservoir, and seal rocks) (Jackson et al., 2015a; Allen et al., 2016).

We focus on the São Paulo Plateau (SPP), Santos Basin, offshore Brazil an area characterized by an intricate pattern of salt diapirs and minibasins formed in response to flow of a thick, layered salt (Fig. 1c) (>2 km, Davison et al., 2012, Fiduk and Rowan 2012; Jackson et al., 2015b). The SPP has a complex, protracted, multiphase salt-tectonic history. It is located at the present-day toe-of-slope, between the somewhat enigmatic and controversial Albian Gap (see below), and a c. 30 km wide salt nappe developed at the downdip end of the basin (Davison et al., 2012; Quirk et al., 2012; Jackson et al., 2015b) (Fig. 1c-d). The deep structure of the SPP is defined by significant base-salt relief related to a Jurassic-to-Cretaceous rift event that defined the early evolution of the margin (Fig. 1d and 2) (Davison et al., 2012; Alves et al., 2017).

The salt-related structure, origin and evolution of the SPP and the neighbouring Albian Gap have been intensely debated over the last few decades. More specifically, this debate centres on: (i) the kinematics of opening of the Albian Gap; and (ii) the kinematic link between the Albian Gap and salt-tectonic structural styles observed on the downdip SPP. Two end-member models have been proposed. The first model states that post-Albian deformation on the SPP was largely driven by regional shortening linked to coeval updip extension (Quirk et al., 2012; Fiduk and Rowan 2012; Guerra and Underhill, 2012; Alves et al., 2017). This extension was accommodated by slip on the Cabo Frio Fault, a large landward-dipping, salt-detached normal listric fault bounding the downdip margin of the 50-60 km wide Albian Gap and its overlying rollover (Fig. 1c-d) (Jackson et al., 2015, figure 5a). In contrast, the second model argues that, after an initial (Albian) phase of modest shortening, the main, post-Albian phase of deformation on the SPP was driven by salt inflation resulting from salt expulsion from beneath the Albian Gap. In this model, the Albian Gap did not form due to *post-Albian extension*, thus any post-Albian contractional deformation on the SPP was linked to some other process (Ge et al., 1997; Jackson et al., 2015b; Dooley et al., 2015; Jackson and Hudec, 2017). The second model does however envisage that *Albian extension* generated a c. 60 km wide salt wall that was later expelled seaward to drive post-Albian contraction on the SPP (Jackson et al., 2015b, figure 5b; Jackson and Hudec, 2017). The evolution of the Albian Gap and SPP are therefore intrinsically connected. Understanding the kinematics of one can improve our understanding of the other.

Pichel et al. (2018) recently described the geometries and 3D kinematics of salt-related asymmetric minibasins on the SPP. These ramp-syncline basins record 28-32 km ($\pm$2 km) of Late Cretaceous-Paleocene basinward translation of salt and its overburden across prominent base-salt relief (cf. Marton et al., 1998; Peel et al., 1998; Jackson et al., 2001; Jackson and Hudec, 2005; Pichel et al., 2019a). Pichel et al. (2018) did *not* however detail the way in which this particular style of salt tectonics related to the overall structural evolution of the SPP in particular, or the Central Santos Basin in general. The question thus remains, “how does this translation relate to and contribute to the debate surrounding the origin of the Albian Gap?”. More generally, we also answer the following questions: 1) what are the main triggers and drivers of salt tectonics on the SPP?; and 2) how does basinward translation of salt and its overburden across pre-salt structures influence the timing and style of diapirism and minibasins?

2. Tectono-Stratigraphic Framework

The São Paulo Plateau is an area of thick Aptian salt that has flowed to form a complex pattern of salt diapirs and anticlines (Fig. 2) (Davison et al., 2012; Guerra and Underhill, 2012; Fiduk and Rowan, 2012; Mohriak et al., 2012; Jackson et al., 2014a,b; 2015b). The pre-salt interval is characterized by NE-oriented graben and half-graben formed during late Barremian-early Aptian rifting. These basins are filled by non-marine clastic strata and overlain by lacustrine carbonates (Meisling et al., 2001; Modica and Brush, 2004; Karner and Gambôa, 2007; Mohriak et al., 2008, 2009; Contreras et al., 2010). During the late Aptian, fault activity ceased on the SPP and a thick (up to 2.6 km) salt layer was deposited (Fig. 2) (Davison et al., 2012). Although salt deposition occurred after active faulting (i.e. it is locally post-rift), relief inherited from the preceding rift phase controlled salt thickness variations; i.e. salt was thin across rift-related footwall highs and thick in intervening hangingwall depocentres (Fig. 2) (Davison et al., 2012; Alves et al., 2017; Rodriguez et al., 2018; Pichel et al., 2018).

During the early Albian, the Santos Basin experienced fully marine conditions due to thermally-induced, post-rift subsidence and a rise in eustatic sea-level. This resulted in widespread deposition of carbonate-dominated succession that is up to c. 200-300 m thick in the study-area (Fig. 1d and 2) (Modica and Brush, 2004). During the late Albian, the basin tilted south-eastward, inducing gravity gliding of the salt and its overburden. Salt-related deformation produced an array of thin-skinned, predominantly seaward-dipping salt-detached normal faults that dismembered the Albian carbonate platform into extensional rafts updip of the study-area (Demercian et al., 1993; Cobbold et al., 1995; Mohriak et al., 1995; Guerra and Underhill, 2012; Quirk et al., 2012). Post-Albian sedimentation was dominated by clastic progradation, with sediments derived from the uplifting of the Serra do Mar mountain range (Modica and Brush, 2004).

3. Methods

This study uses a zero-phase processed, time-migrated, 3D seismic reflection dataset that covers 20,122 km^2 of the SPP, Central Santos Basin, Brazil (Fig. 1c). Inline (west-east) and crossline (north-south) spacing is 18.75 and 25 m, respectively. Vertical sampling interval is 4 ms two-way time (ms TWT) and the total record length is 5500 ms TWT. The survey display follows the Society of Economic Geologists (SEG) normal polarity, where a downward increase in acoustic impedance is represented by a positive reflection event (white on seismic sections) and a decrease in acoustic impedance by a negative event (black on seismic section) (Brown, 2011). The average dominant frequency in the Aptian salt is c. 36 Hz and the interval velocity is c. 4400 m/s, yielding a vertical resolution of c. 29 m (Rodriguez et al., 2018). Overburden strata have a dominant frequency that decreases (from c. 40 Hz to c. 31 Hz) and an average velocity that increases (c. 1900-2015 m/s) with depth, yielding a vertical resolution of c. 12-17 m. Horizontal resolution is twice the seismic line spacing (i.e., 37.5 m in the E–W direction and 50 m in the N–S direction) (Jackson et al., 2015b). We also use three PSDM (pre-stack depth-migrated) seismic lines that are c. 350 km long and trend broadly parallel to the bulk tectonic transport direction (i.e. NW-SE). These lines allow us to place our relatively local observations in their regional context (Fig. 2).

We mapped salt structures and minibasins in three-dimensions using the approach described in in Pichel et al. (2018). Key seismic stratigraphic surfaces (Fig. 2) were identified using the well control outlined in previous publications (Guerra and Underhill, 2012; Jackson et al., 2015b; Rodriguez et al., 2018). A base-salt (BoS static-corrected map, see Pichel et al., 2018; fig. 3) was used in order to determine the orientation and relief of pre-salt topography, and its spatial (and possibly kinematic) relationship with the salt and supra-salt structure.

4. Pre-salt structures

The SPP is defined by two large pre-salt highs: the NNE-oriented Sugar-Loaf Sub-High in the south; and the NE-oriented Tupi Sub-High in the north (Mohriak et al., 2012, Rodriguez et al., 2018). These highs are connected by an ENE-oriented structural high(Fig. 3a) and are part of a larger rift-related structure known as the Outer High (Fig. 3) (Demercian et al., 1993; Mohriak et al., 1995; Davison et al., 2012). The Sugar-Loaf and Tupi sub-highs are bound by large (c. 0.9-1.8 km throw) NNE-SSW-to-NE-SW-striking normal faults; these structures strike roughly perpendicular to the main direction of salt-detached, gravity-driven transport (i.e. ESE to SE; Davison et al., 2012; Quirk et al., 2012; Pichel et al., 2018).

The base of salt is typically undeformed, although it is locally offset by a few relatively small (up to 100 ms TWT or c. 450 m of throw) faults. Where closely spaced, the cumulative throw across these faults controls the development of base-salt ramps and monoclinal geometries at the edge of the largest pre-salt highs (Fig. 2) (Davison et al., 2012; Alves et al., 2017; Rodriguez et al., 2018). This indicates that pre-salt structures and related topography were present before and during salt deposition, with only minor, reduced fault activity during (or after) salt deposition (Davison et al., 2012). Pre- and possibly syn-salt faulting resulted in non-uniform salt deposition, with thicker (>2 km), more halite-rich and thus more mobile salt over pre-salt lows, and thinner (c. 1 km), relatively halite-poor and thus less mobile salt over adjacent highs (Davison et al., 2012; Rodriguez et al., 2018).

The Tupi Sub-High is c. 20 km wide and has a maximum structural relief of 0.9 s (1.5-2 km). It is limited on its basinward (i.e. SE) margin by a steep, basinward-dipping base-salt ramp that is defined by series of SE-dipping pre-salt normal faults (Fig. 2). The landward (i.e. NW) side of the Tupi Sub-High is broadly unfaulted and dips gently landward (Fig. 3). Its northern margin is defined by a steep, NW-oriented edge that changes abruptly to a narrower (10 km wide), NNW-oriented horst (horst-block, fig. 3a; H2 of Alves et al., 2017, fig. 3c). Two smaller, NE-orientated base-salt highs lie 10 and 15 km downdip of the Tupi Sub-High, with another ramp lying c. 4 km to the NE (Fig. 3). These structures define tilted fault-blocks that are up to 5 km wide and have a maximum structural relief of c. 0.6 s (c. 1.2 km). Another broader, semi-rectangular, horst-like high (H4 of Alves et al., 2017, fig. 3c) lies 10 km downdip of the centre of the Tupi High (Fig. 3a-b).

The Sugar Loaf Sub-High is broader (45-50 km) than the Tupi High. Its landward margin is defined by several landward-dipping faults that produce two landward-dipping, base-salt ramps with c. 0.5 s (c. 1 km) of relief (Fig 3). Its basinward edge is characterized by several closely-spaced, basinward-dipping faults defining a single, basinward-dipping, base-salt ramp with c. 1 km of relief (Fig. 3). The trend of the Sugar Loaf Sub-High changes along-strike from NNE in the south to NE in the north. At its northern end it branches into a smaller NE-oriented horst, and the ENE-oriented high that connects it to the Tupi Sub-High further north (Fig. 3a-b).

5. Salt and overburden structures

The SPP is defined by a complex network of salt diapirs and anticlines (Fig. 4) (e.g. Davison et al., 2012; Guerra and Underhill, 2012; Quirk et al., 2012; Jackson et al., 2015b). Diapirs consist mainly of curvilinear salt walls (Fig. 4). Salt structures and (elongate) minibasins trend broadly sub-parallel to the underlying, broadly NE-oriented pre-salt structures in the south and central portions of the study area; further N and NE, salt structures have a more polygonal pattern (Figs. 3-4) (Guerra and Underhill, 2012; Jackson et al., 2015b). In order to explain the distribution of different salt-related structural styles, we divide the area into six domains according to salt and overburden geometries, and the kinematics of the contained structures and their relationship to the base-salt geometry (Figs 3-4).

5.1. Domain I: West of Sugar Loaf

Description

Domain I is located on the gently landward-dipping western edge of the Sugar Loaf High. It is characterized by a NE-oriented salt-cored fold-belt that formed above thick salt (c. 2km on average; fig. 4). Curvilinear salt walls and minibasins in the fold-belt display variable orientations (Figs. 3, 4 and 5). Salt-cored folds trend mainly NE, curving gently northwards to a NNE trend, sub-parallel to the updip edge of the Sugar Loaf High (Figs. 3-5). The folds are 4-15 km long, 1-3 km wide and with wavelengths of 3-5 km (Figs. 4-5). They have rounded to sinusoidal profiles, with occasional box-fold geometries, and are predominantly upright with little or no preferred sense of vergence (Fig. 6a-c). The folds are commonly cored by landward-dipping intra-salt reverse shear zones and cut at their crests by pairs of inward-dipping normal faults (Fig. 6a-c, appendix fig. a). These faults lack associated growth strata and are, thus, inferred to have formed to accommodate outer-arc extension around the fold hinge (Fig. 6a-c); indicating these folds are driven by lateral shortening. Growth synclines in the fold-belt are also curvilinear, trending mainly NE (Figs. 4-5). These depocentres are relatively symmetric, thin (c. 200-500 m) and narrow (1-4 km, fig. 6a).

The easternmost (i.e. basinward) folds formed during the Late Cretaceous to early Paleocene as shown by growth strata of equivalent age onlapping a tabular and thus pre-kinematic Albian unit. Further westward (i.e. landward), fold growth commenced later (i.e. mid Late Cretaceous) as indicated by the tabular, pre-kinematic section becoming thicker and incorporating post-Albian strata (sub-vertical white lines; Figs. 6a-c). Most folds became inactive in the early Paleocene, although most landward folds were active until the late Paleocene, before being mildly rejuvenated during the Neogene (Fig. 6a-c).

In a few cases, especially over base-salt flats, minor reactive diapirism and wall formation is seen in association with inward-dipping and younging normal growth faults cutting the crests of some folds. The development of these structures suggests minor late-stage extension (Fig. 6a-c). These reactive walls are flanked by a broadly isopachous Albian interval that is upturned and offset by outer arc extension-related normal faults (i.e. without syn-sedimentary growth). These geometries are similar to the adjacent salt-cored folds, suggesting the walls may have been initiated at the same time by the same process (i.e. in response to Late Cretaceous shortening), with the normal growth faults reflecting later (i.e. latest Cretaceous to early Paleocene), relatively minor, reactive diapirism (Fig. 6a-b). In some cases, the walls are overlain by a c. 600 m thick, extensionally thinned Paleocene roof (Fig. 6b), suggesting Neogene active diapirism and uplift, probably associated with mild regional shortening.

Tall (up to 4.9 km), curvilinear and variably oriented salt walls, mostly trending NNE-WNW (Fig. 6d), occur at the northern edge of Domain I. These walls bound large, thick minibasins underlain by relatively thin salt and likely locally welded (figs 4-5 and 6d). These minibasins are relatively symmetric in cross-section, being thicker in their centre where top-salt and, occasionally, top-Albian lie below the dataset (Fig. 3a). Thinning and onlap of latest Cretaceous/Paleocene strata onto an upturned Albian/Upper Cretaceous collar that is extended by inward-dipping normal growth faults indicates that bounding salt walls initially rose due to latest Cretaceous to

Paleocene extension (Fig. 6d). Mild Albian-Late Cretaceous growth also occurred as shown by minor thickness variations and local intraformational unconformities within strata of this age directly adjacent to the salt wall (Fig. 6d). These walls are still growing, being driven by post-Paleocene load-driven subsidence and salt expulsion due to the ponding of anomalously thick (400-600 m) mass-transport complexes (MTCs) and, secondarily, by mild extension (Fig. 6d).

Interpretation

The most prominent structural element in Domain I is a landward-younging fold-belt that is oriented sub-parallel to a landward-dipping base-salt ramp defining the updip edge of the Sugar Loaf High (Fig. 6). Landward-dipping intra-salt shear zones in the centre of the salt-cored anticlines suggest lateral salt flow (see Pichel et al., 2018) was associated with viscous shear drag within the salt (i.e. Couette flow) and that deformation was mainly driven by lateral shortening. Shortening occurred as basinward-flowing salt and overburden was buttressed against the Sugar Loaf High, promoting salt inflation and overburden contraction (cf. modelling results of Dooley et al., 2016 and Pichel et al., 2018; 2019b). Extension and reactive diapirism at the crests of some anticlines appears spatially related to areas where the base-salt is relatively flat. We therefore suggest that extension occurs due to acceleration of salt and its overburden downdip of the buttress (cf. physical models of Dooley et al., 2016; Pichel et al., 2019b). The Domain I fold-belt is part of the major translation system identified by Pichel et al. (2018), and its evolution is strongly linked with Domain II further basinward (see below).

5.2. Domain II: Sugar Loaf Sub-high

Description

The Sugar Loaf High is dominated by long (35-50 km), wide (6-12 km) salt walls and flanking minibasins (Figs. 3-5). A few NE-oriented, salt-cored folds also occur at the boundary between domains I and II, where they are situated above or landward of base-salt landward-dipping ramps defining the updip edge of the Sugar Loaf High (Figs. 3-4)

Salt walls (1-3, figs. 4-5) have a dominant N-NNE orientation, parallel to the Sugar Loaf High, whereas those located further basinward trend NE, sub-parallel to the ENE pre-salt high downdip (Figs. 3-5). These walls have complex cross-sectional geometries, being characterized by: a) direct onlap onto, and thinning and significant upturn of Albian strata against the diapir flanks, usually near their centre where they are wider (e.g. wall 3, fig. 7a), or; b) by sub-horizontal to only moderately upturned and tabular Albian strata, which is extensionally thinned by inward-dipping, Late Cretaceous-early Paleocene normal growth faults (e.g. walls 2 and 4, fig. 7a and walls 2 and 3, fig. 7b-c). In both cases, Albian-Upper Cretaceous strata are completely separated by diapirs, and the overlying Upper Cretaceous/early Paleocene interval is characterized by landward-thickening and younging strata contained in ramp-syncline basins (RSBs, fig. 7a-c; appendix fig. i), which form by basinward translation over base-salt ramps (Jackson and Hudec, 2005; Pichel et al., 2018).

On the eastern flanks of walls 1-4 in Domain 2, strata at the base of the ramp-syncline basins onlap an Albian/Cenomanian section (yellow arrows, figs. 7d-e). The tops of the ramp-syncline basins are erosionally truncated (red arrows, figs. 6d-e) towards the western flank of a basinward salt wall (Fig. 7a-c). Strata in the upper parts of the ramp-syncline basins directly onlap bounding salt walls and are extended by inward-dipping normal faults of broadly similar same age (e.g. latest

Cretaceous to early Paleocene; RSBs 1b and 2a-b, fig. 7a-e). These normal faults suggest an extensional origin for these of salt walls and synchronous extensional deformation of adjacent ramp-syncline basins (eastern flank of walls 1-2, fig. 7a and 7d and walls 2-3 in fig. 7b-c and 7e; and triangular diapirs of figs. 7f-g).

Salt walls display along-strike variations in cross-sectional geometry. Near their low-relief ends, where growth starts later (mid-Late Cretaceous, fig. 7f), they are triangular. In contrast, near their centres, where they started growing earlier (i.e. Albian-Cenomanian) they are wider and taller, and have approximately flat-tops, present strongly upturned flank strata, and contain complex intra-salt deformation (walls 2-4, fig. 7a-c) (Jackson et al., 2014; 2015). At their low-relief ends, narrow triangular diapirs overlie broader, more rounded salt structures enveloped by mildly upturned Albian-Upper Cretaceous strata that are extensionally thinned by inward-dipping normal faults at their flanks (2 and 3, fig. 7f-g and appendix fig. d). These diapirs are surrounded by gentle anticlines of similar age, suggesting the former formed by reactive piercement of the crest of salt-cored anticlines whose roof was thinned by erosion and/or outer-arc extension (cf. Domain I; figs. 5 and 7f-g).

Interpretation

The geometries described above indicate that the largest walls in Domain II initially formed in response to a local, relatively early (i.e. Albian) phase of active rise (central part of wall 3, figs. 4 and 7a). A later, more protracted (Late Cretaceous-Paleocene) period of diapir growth was associated with basinward translation of salt and overburden, which coincided with the development of ramp-syncline basins (cf. Pichel et al., 2018). Walls started growing later (mid-Late Cretaceous onwards) at their northern and southern terminations; because of this, these younger portions present a simpler evolution that can be used to help understand the more complex and sometimes incomplete tectono-stratigraphic record preserved at their centres. Their spatial relationship to intra-salt reverse shear zones and sub-parallel trains of salt-cored folds indicate the walls were affected by at least one phase of shortening (Jackson et al., 2015b). Intra-salt shortening, however, cannot fully account for all the complex intra-salt deformation observed in Domain II (Jackson et al., 2015b; Dooley et al., 2015).

Differences in the geometry of the Albian (i.e. faulted and upturned against the flanks of diapirs) and Upper Cretaceous/Paleocene strata (i.e. only mildly deformed adjacent to and directly onlapping the diapirs) contained within the ramp-syncline basins suggest shortening occurred immediately post-Albian. The presence of inward-dipping normal faults above triangular, reactive diapirs at the low-relief ends of these walls, however, suggest shortening and/or active rise was followed in the Late Cretaceous-Paleocene by local extension (Fig. 7f-g). Faulting and reactive rise of the diapirs further thinned their roofs, allowing active piercement and eventual passive growth of the diapirs as they reached the seafloor (walls 2-4, fig. 7a-c) at their centres. Where they had reached the seafloor to form passive diapirs, any subsequent extension was accommodated mostly by diapir widening. Thus, the salt walls development involved an initial phase of shortening-driven active rise followed by reactive and passive rise with diapir widening at their centres (walls 2-4, fig. 7a-c). At their low-relief ends, growth was driven by buckle-folding followed by reactive diapirism (walls 2-3, fig. 7f-g).

The coeval development of ramp-syncline basins and multistage deformation in Domain II and a salt-detached fold-belt in Domain I, are consistent with physical (Dooley et al., 2016, 2018) and numerical models (Pichel et al., 2018, 2019b) of salt and overburden translation over landward-dipping base-salt ramps. A conceptual kinematic model based on seismic examples from the study-area illustrates the structural evolution of these two domains (Fig. 8). As salt moves from an area of thick salt updip to thin salt over the base-salt high, the flux mismatch results in inflation against its landward-dipping ramps and development of a ramp-syncline basin basinward above base-salt flats (Fig. 8a-b, phases I-II). An earlier thinned roof (phase I) allows salt to rise within an active diapir (Fig. 8a, phase II), whereas an earlier tabular roof (phase I) results in less salt rise and development of buckle-folds (Fig. 8b, phase II). The system becomes partially pinned over the ramps resulting in asymmetric growth, i.e. increased inflation and uplift on the landward side, and extension and/or widening of the basinward side over the base-salt plateau (Figs. 7a-c and 8, phase III). This occurs because as salt gradually thickens, basal-drag is reduced and salt accelerates, reversing strain-patterns after an initial phase of inflation over the base-salt flat (Dooley et al., 2016; 2018). This acceleration and continuous salt thickening causes the salt structure to leave the ramp, moving over the base-salt plateau whilst a new buckle-fold develops over the landward ramp, and a new ramp-syncline basin over the intermediate base-salt flat (Fig. 8a-b, phase IV). In the case of an earlier active diapir, continuous inflation allows the diapir to reach the surface; subsequent extension is cryptic and accommodated by diapir widening (Fig. 8a, phase III), which explains the >10 km wide walls over the Sugar-Loaf High and why they are wider where growth started earlier (Albian) (walls 2-4, figs. 3-4 and 7a-c). In the case when the early structure is a salt anticline (phase II, fig. 8b), a reactive diapir nucleates at its extensionally thinned crest (triangular diapirs in figs. 7f-g and 8b, phase III). Because they form over inflated salt beneath a relatively thin, syn-kinematic overburden, these reactive diapirs are symmetric (Jackson and Hudec, 2017).

5.3. Domain III: North edge of Sugar Loaf Sub-high

Description

Domain III is located at the northern edge of the Sugar Loaf High, where it splits into a NNE-oriented horst, and the ENE-oriented high that connects it to the Tupi Sub-high (Fig. 3). This domain is characterized by a change in the orientation and plan-form geometry of salt structures and adjacent minibasins relative to domains I and II. A 10 km wide, NNE-oriented salt wall (5, figs. 4-5 and 9), which is roughly rectangular in plan-view, occurs above the NNE-oriented, pre-salt horst. This southern margin of wall 5 has a sharp triangular edge where it is linked to a NE-oriented wall (3, figs. 4-5) in Domain II via a narrow (<1 km) NW-oriented, extensional wall. At its northern end wall 5 splits into two curved, narrow (3-4 km) NE-oriented walls (walls, 5a-b, figs. 4-5). Further basinward in Domain III, walls are dominantly ENE-oriented (c.f. wall 6, figs. 4-5), sub-parallel to the ENE high downdip. These walls have similar cross-sectional profiles to those in Domain II, being flanked by an upturned collar of a broadly tabular, highly faulted Albian section that is onlapped by Late Cretaceous-early Paleocene strata contained in ramp-syncline basins. The latter is deformed and extensionally thinned by inward-dipping growth faults at their edges (Wall 5, fig. 9).

Downdip of the smaller horst-block, a roughly rectangular, 8-10 km wide ramp-syncline basin overlies a basinward-dipping base-salt ramp, being bound downdip by a 6 km wide, ENE-oriented sigmoidal wall that itself partly overlies the ENE-oriented, pre-salt high (Wall 6, figs. 3-5) This wall shows signs of Late Cretaceous-Paleocene extension at its northern end, being triangular in cross-section and flanked by inward-dipping normal faults (wall 6, fig. 9a). However, at its central and southern end it shows evidence of seemingly simultaneous shortening in the form of folding, inflation and intra-salt reverse shearing (wall 6, fig. 9b-c).

Interpretation

Salt walls in Domain III have similar cross-sectional profiles and relationships to base-salt relief as those in Domain II, suggesting they have a similar cross-sectional evolution (i.e. Late Cretaceous shortening-driven active diapirism followed by widening associated with reactive and passive rise during the latest Cretaceous-Paleocene) (Fig. 7, see section 5.2.). However, their complex plan-view arrangement, defined by changes in orientation, the presence of highly-oblique walls, and sigmoidal plan-view shapes associated with marked along-strike variations in profile, suggests differential translation, plan-view rotation, and perhaps even shearing at the edge of the Sugar Loaf Sub-High (Figs. 9-11).

As salt and its overburden translated downdip and reached the NNE-oriented horst-block at the edge of the Sugar Loaf Sub-high, convergent salt flux resulted in thickening and pinning over the horst; whereas further northwards the system continued to translate downdip, unimpeded by pre-salt relief (Fig. 9). Differences in the rate and magnitude of downdip salt flow caused plan-view rotation and possibly shearing. Wall 5 rotated counter-clockwise as it was temporarily pinned parallel to the base-salt topography of the NNE-oriented horst-block. Structures located further to the north and basinward (walls 5a, 5b and 6), away of the NE-oriented pre-salt horst, rotated clockwise as they were located in areas were salt was flowing basinward faster (Fig. 9).

Wall 6 and another smaller wall further north were squeezed at their southeast flank, which are located over a landward-dipping base-salt ramp (fig. 9b). In contrast, on their northern edges away from the base-salt relief, they were translating basinward faster and were thus extending in those locations (Fig. 9a and 10). This differential flow resulted in plan-view shearing and development of sigmoid-shaped walls (Fig. 10). Physical models simulating translation across discontinuous pre-salt highs (cf. Dooley et al., 2018) illustrate how salt flow changes and diverges around these structures, producing considerable rotation and shearing of salt walls and development of similar sigmoidal geometries (Figs. 11a-b).

5.4. Domain IV: West of Tupi

Description

Salt walls in Domain IV trend NE and are up to 4.9 km tall, 30-50 km long, 5-8 km wide and highly arcuate, and are connected by shorter (4-8 km long) and narrower (>1.5 km) NNW-to-NW-oriented walls (Figs. 4-5). The larger, NE-oriented walls are flanked by relatively thin (c. 200-300 m) Albian growth strata abruptly thinning towards, directly onlapping onto, and being intensely upturning against the wall (walls 7-8, fig. 12a-b). More significant thickness variations occur within overlying Upper Cretaceous to mid-Paleocene strata filling c. 4 km thick minibasins (Fig. 12). These strata onlap upturned Albian strata or abut directly onto the salt walls (Fig. 12a-b). The minibasins are generally characterized by vertically-aligned depocentres (i.e. bowls *sensu* Rowan and Weimer, 1998) and raised bathymetric rims (*sensu* Hudec et al., 2009) (Fig. 12a-b, appendix fig. e). This indicates that, in contrast to other minibasins that are essentially ramp-syncline basins (Domains II-III and V-VI, see below), minibasins in Domain IV formed primarily by loading and density-driven subsidence. In some cases, the minibasins are tilted and present a wedge-shaped mid-Paleocene section that may be contained in an asymmetric turtle anticline. The latter geometry likely formed in response to early-mid Paleocene minibasin welding (*sensu* Rowan and Weimer, 1998) (Fig. 12a-b). The associated NE-oriented walls were also affected by mild extensional collapse during the Late-Paleocene-Neogene, although the wall located furthest basinward at the updip edge of the Tupi High kept growing by active rise (wall 11; Fig. 12a-b).

The narrower, NW-oriented walls linking walls 9 and 10 are triangular in cross-section and flanked by inward-dipping and younging, Upper Cretaceous to Paleocene normal faults (Fig. 12c, appendix fig. c). A geometrically similar, albeit wider and taller wall located further north, connects walls 8 and 9. Albian strata on its flanks are capped by a top-Albian erosional unconformity, denoting late Albian active rise (Fig. 12d). Overlying, Upper Cretaceous strata thin and onlap directly onto this wall and are unfaulted, whereas younger Paleocene strata define a turtle anticline that is locally deformed at its crest and immediately next to the diapir, by inward-dipping and younging normal faults (Fig. 12d). An earlier WNW-NW Albian trend characterized by narrow (>1 km), low-amplitude (>250 m) anticlines and growth synclines, capped by a top-Albian unconformity, occur within and at the bases of the larger NE minibasins at the north-northeast portion of Domain IV (Figs. 4 and 12d).

Interpretation

Highly-upturned Albian growth strata along the wall flanks constitute basal flaps that likely deposited when the original salt contact dipped gently, allowing a wedge of strata to directly onlap a low-relief diapir (cf. Rowan et al., 2016; Jackson and Hudec, 2017). This indicates an earlier, relatively minor phase of Albian salt flow driven by halokinesis (i.e. passive and/or active rise) followed by late Albian partial burial.

During the Late Cretaceous, after breaking through their thin Albian roof and reaching the surface due to continuous halokinetic rise, these walls experienced a protracted phase of load-driven passive rise (i.e. downbuilding) that continued until the middle Paleocene (Fig. 10a-d) (Jackson et al., 2014b; 2015a). Brief phases of active rise occurred during the latest Cretaceous as seen by relatively greater upturn of equivalent-age strata and the local development of outer-arc stretching-related faults (walls 8-9, fig. 12a-b) (*sensu* Rowan et al., 1999). By the middle of the Paleocene, the walls became partially buried; they continued to grow however by vertical load-driven rise as suggested by their bathymetrically-raised rims (*sensu* Hudec et al., 2009) (walls 7-8).

In the north, where they sit above a pre-salt high, salt walls 10 and 11 (fig. 12a-b) rise reactively due to overburden stretching (Fig. 12a). In contrast, to the south, where it lies landward of the same high (Fig. 5), salt wall 10 rises and uplift a c. 400 m thick roof (Fig. 12b), which implies active diapirism driven by shortening. In general, downdip walls near the Tupi High (9-11) are affected more and earlier by regional stresses (compression and/or extension) than walls further updip (walls 7-8, figs. 12a-b). These stresses are expressed by the formation of inward-dipping normal faults that deform the sub-horizontal strata flanking reactively rising walls (walls 10-11, fig. 12a). Normal faults also accommodate widening of walls undergoing extension-driven collapse (walls 8-9, figs.12a-b).

Domain IV is located next to Domains II and II, both of which provide clear evidence for downdip translation. It is therefore likely that Domain IV also translated downdip.

However, the lack of base-salt relief in Domain IV results in deformation being markedly different, i.e. deformation controlled by sedimentary load-driven subsidence and salt expulsion, and passive diapirism (Figs. 5 and 12). As structures located downdip in Domain IV approached the Tupi Sub-high (walls 9-11, fig. 12a-b), they were however affected by plan-view differential flow and cross-sectional salt flux variations related to the base-salt relief. Updip walls (7 and 8, fig. 12a-b) were less affected by these processes because they were farther (c. 50-60 km) from the Tupi Sub-high.

NW-oriented reactive (i.e. extensional) walls at the southern edge of Domain IV formed due to plan-view divergent flow as salt and its overburden translated faster basinward to the north, away from the Sugar Loaf High (Figs. 3, 4 and 12c). Narrow, NW-oriented Albian anticlines within large minibasins in the north of Domain IV may have formed by S-SW-directed shortening associated with the concave geometry of the northern basin margin (c.f. Cobbold et al., 1995). Development of this hypothesis requires integration with additional published data from north of the present study-area; this will be done in the discussion (see below).

5.5. Domain V: Tupi High

Description

The Tupi High dominates Domain V, and is defined by a gently landward-dipping base-salt ramp that passes abruptly downdip into a steeply basinward-dipping ramp (Fig. 3 and 13a-b). Domain V is characterized by large (30-40 km long by 2-4 km wide), curvilinear salt walls and anticlines that mainly trend NE-NNE. Large walls are linked by smaller NW-oriented walls, locally creating a crude polygonal pattern (Fig. 3-4).

On the west flank of the Tupi High, on the gently landward-dipping base-salt ramp, NE-oriented salt structures are predominantly characterized by low amplitude (c. 300 m) anticlines. These structures are occasionally cored by seaward-verging, intra-salt reverse shear zones, and are typically capped by a broadly tabular, folded Albian roof that is onlapped by Upper Cretaceous-to-Paleocene strata (Fig. 13a-b). 5-10 km further basinward, where the base-salt is relatively flat (Fig. 13b), similar salt anticlines are more heavily faulted, having their roofs completely dismembered and pierced by reactive diapirs (Fig. 13a-b, appendix fig. b). These geometries suggest structures were originally formed by contraction as salt-cored buckle-folds and then later reactivated by regional extension, as in Domain I (see section 5.1).

Further basinward, approaching the crest of the Tupi High (Fig. 13c), new sets of shear zone-cored buckle folds appear where the base-salt steepens. These folds are capped by tabular Albian-early Upper Cretaceous roofs that are dissected by outer-arc extension-related normal faults and onlapped by thin, Upper Cretaceous growth strata truncated above by a top Cretaceous unconformity (Fig. 13c). The tabular, pre-kinematic interval (white lines, fig. 13c) thickens gradually landward, suggesting shortening commenced later there, and that overall, contraction propagated landward from the crest of Tupi Sub-high. Folds at or near the crest of the structure (the *extensional hinge* of Dooley et al., 2016) are relatively more stretched, resulting in roof dismembering by normal faulting and minor reactive rise (Fig. 13c-d, appendix fig. a-b). Where they lie directly above the crest of the Tupi High or its base-salt basinward-dipping ramp, folds are more open or monoclinal (Fig. 13c-d). Their flanks are sub-parallel to the base-salt, being deformed by predominantly basinward-dipping normal faults and onlapped by Paleocene strata contained in ramp-syncline basins (RSB 5, fig. 13c-d).

Downdip of the Tupi High (the *contractional hinge* of Dooley et al., 2016), above a set of closely-spaced tilted fault-blocks (Figs. 3-5), deformation is again dominated by salt-cored folds (Fig. 13a-e). The fold-belt is defined by 1-2 km wide and 10-20 km long, NE-oriented curvilinear folds that are of higher amplitude (500-700 m) and frequency (1-3 km) than those immediately updip or in Domain I (Figs. 4-5 and 11). The pre-kinematic interval consists mainly of tabular Albian strata, occasionally thinned by outer-arc extensional faults and/or local erosional unconformities (Fig. 13a-e). The sense of vergence immediately downdip of the Tupi High is more variable than in Domain I, with seaward- and landward-verging folds and thrusts being equally common (Fig. 13a-e). Folded Albian strata are capped and onlapped by Upper Cretaceous-Paleocene strata contained in stacked ramp-syncline basins (c.f. Pichel et al., 2018) (RSBs 3-5, figs. 13a-b and d)

Supra-salt thrusts cut the steeper flanks of tight, asymmetric anticlines. In many cases, diapiric piercement of the overburden locally occurs as a sliver of salt is carried up in the hangingwall of the supra-salt thrusts (thrust piercement; cf. Hudec and Jackson, 2006) (Figs. 13a-e; appendix fig. h). Narrow (<1 km), NE-oriented walls also form by squeezing and salt injection into extensionally and/or erosionally thinned roofs of salt-cored folds (fold injection; cf. Beloussov, 1959; Dooley et al., 2015; Jackson and Hudec, 2017) (Fig. 13d, appendix figs. g-h). Many folds are cored by intra-salt shear-zones, and are associated with intense upturn and structural thinning of sub-vertical Albian and Upper Cretaceous strata (Fig. 13a-d). In places, these walls are capped by small salt tongues associated with thrust piercement, which, in places, can be double-vergent (Fig. 13d, appendix figure table). NW-oriented walls form at the edges of NE-oriented folds and/or where salt walls converge along-strike (Figs. 4-5). The NW-oriented walls are located within base-salt lows and are characterized by thicker salt than adjacent areas comprising NE-oriented salt structures and stacked, seaward-verging, reverse intra-salt shear zones (Fig. 13c and f).

Interpretation

The presence of a fold-thrust-belt, ramp-syncline basins and squeezed diapirs suggest Domain V was characterised by basinward translation of salt and its overburden across closely spaced sets of tilted fault-blocks defining gentle landward-dipping and steep basinward-dipping, base-salt ramps (Fig. 14a) (Dooley et al., 2018; Pichel et al., 2019b). More specifically, convergent salt flux and buttressing over a gentle landward-dipping ramp resulted in contraction and formation of a landward-younging fold-belt (Fig. 13a-c and 14a). When these folds translated downdip onto a relatively narrow (~5 km) base-salt flat, they were mildly extended, similar to the ones presently located above base-salt flats in Domain II (phase IV, fig. 8b).

Over the basinward-dipping ramp at the edge of the Tupi High, the cross-sectional area of salt arriving at its crest was smaller than the one leaving. This produced a flux mismatch and, consequently, formation of a near-monoclinal zone of cover subsidence and a ramp-syncline basin above the ramp (Figs. 13 and 14a). The updip part of this ramp-syncline basin, directly above the top of the ramp, was characterized by extension, whereas contraction occurred above and downdip of the base of the ramp (Fig. 13 and 14) (extensional and contractional hinges, respectively, cf. Dooley et al., 2018; Pichel et al., 2019) Extension over the crest of the Tupi High partly unfolded salt anticlines that formed further updip; the degree of extension was however minor when compared to the significant amount of contraction (i.e. thrusting and diapir squeezing) occurring further downdip (Fig. 13 and 14a). This occurred as the set of closely-spaced pre-salt tilted fault-blocks (Fig. 3) produced abrupt flux variations and buttressing of salt flow, resulting in pulses of renewed contraction. This contraction overprinted any earlier-formed extensional structures, amplifying earlier formed salt-cored folds, squeezing (and almost welding) pre-existing diapirs, and generating overburden thrusts and local diapiric injection of fold hinges (Figs. 13 and 14a).

We infer that NW-oriented walls show an even higher degree of contraction and are of higher relief than cross-cutting, NE-oriented walls (Fig. 14c and f) due to plan-view variations of salt flow, and divergence of salt flow around discontinuous base-salt structures (Fig. 14b). This is explained by the concave-into-the-basin plan-view geometry of the downdip edge of the Tupi High and the presence of a pre-salt horst immediately downdip of its centre (Figs. 3 and 14b). As salt anticlines translated downdip from the crest of the Tupi High they were pinned behind this horst, converging and thus coalescing, and thereby producing thicker, NW-oriented walls. These anticlines also rotated as they were locally pinned at their ends by the base-salt relief (Figs. 14b), similar to that observed in physical models (Fig. 11a-b) (Dooley et al., 2018).

5.6. Domain VI: NNW branch and N of Tupi

Description

Domain VI lies above and downdip of the NNW-oriented horst forming part of the northern extension of the Tupi High (Fig. 3). This domain is dominated by NNE-oriented salt anticlines and walls, with a few WNW-oriented walls (Figs. 3-5). The structural pattern becomes progressively more polygonal to the north, away from the pre-salt highs, due to an increasing number of WNW- and NW-oriented salt walls (Fig. 4). Flanking Albian strata gradually thin towards and directly onlap the salt walls, and are capped by local unconformities (TA unconformities, fig. 15) at their flanks, indicating an early, Albian phase of growth. WNW-oriented anticlines at the base of large minibasin in the west of Domain VI are geometrically similar to those in the adjacent Domain IV, probably indicating they formed at the same time in response to the same process (i.e. SW-directed Albian shortening, see section 5.4, figs. 4 and 12d).

Landward, above the NNW-oriented pre-salt horst-block, the structural style is dominated by wide (3-5 km), NNE-oriented, triangular salt walls, whose roofs are cut by numerous inward-dipping and -younging normal growth faults (walls 13 and 14, figs. 4-5 and 15a). These walls have gentle to moderately-dipping flanks that were extended by normal growth faults during the Late Cretaceous-early Paleocene, indicating they formed by reactive diapirism (reactive diapirs, fig. 15a). They are bound on their basinward edges by c. 500 m thick ramp-syncline basins of same age (RSBs 6 and 7, fig. 15a), indicating extension occurred in tandem with translation, after an initial (Albian-Cenomanian) phase of salt inflation/active rise. Above the basinward-dipping edge of the horst, a Paleocene salt anticline and wall uplift and fold an Upper Cretaceous ramp-syncline basin which is itself onlapped by strata contained in a younger, early Paleocene ramp-syncline basin (stacked RSBs 6-7, fig. 15a-b; cf. Pichel et al., 2018), indicating early Paleocene contraction.

Further basinward, downdip of the NNW-oriented pre-salt horst, the deformation style is notably different, being represented by a 30 km wide, NNE-NE-oriented fold-belt. In addition to displaying a different trend to those further updip, these folds mainly grew during the Late Cretaceous-Paleocene (as opposed to the Albian). This is demonstrated by a predominantly isopachous Albian interval that is onlapped by Upper Cretaceous-Paleocene contained in a ramp-syncline basin (6, Fig. 15a). The Domain VI fold-belt displays a similar spatial relationship to base-salt structure as the one in Domain V, being developed just downdip of an underlying pre-salt high. Furthermore, this fold-belt has a similar overall geometry to the one developed in Domain V (Fig. 13-14a), although the degree of intra-salt shearing, diapir squeezing and thrusting is markedly less, with fewer salt walls rising diapirically from the top of salt-cored anticlines (Fig. 15a).

Northwards, away from the pre-salt high, walls are of higher relief (2-3 km) than the ones further south, being surrounded by equally thick, nearly-welded minibasins. The walls are flanked by highly upturned, Albian to Upper Cretaceous strata that directly onlap the walls and thicken into flanking minibasins (Fig. 15c). More weakly deformed Paleocene strata onlap the Upper Cretaceous carapace and cap flanking diapirs; these strata also show less pronounced thickness variations than the underlying strata (Fig. 15c). Both Upper Cretaceous and Paleocene strata are cut by normal faults that overlie the salt walls; these faults are best-developed on the flanks of triangular diapirs and are associated with local syn-depositional growth (i.e. strata below regional, dashed white lines, fig. 15c), indicating lateral extension. However, in cases where normal faults occur over the wall crest but *without* growth strata, we infer they formed in response to outer-arc stretching during roof uplift and bending driven by active diapirism. These characteristics indicate early (i.e. Albian to Late Cretaceous) deformation is controlled by load-driven subsidence and downbuilding (i.e. passive diapirism), followed by minor extensional growth (early Paleocene reactive diapirism) and then later (Paleocene-Neogene), halokinetic active rise (Fig. 15c).

Interpretation

Domain VI was subjected to significant downdip translation of salt and its overburden as evidenced by the presence of large ramp-syncline basins (Figs. 13 and 15). South of Domain VI, horizontal translation and the associated development of salt structures were strongly influenced by base-salt relief associated with the NNW extension of the Tupi Sub-high (Fig. 15a); further northwards, away from this high, structures formed mainly in response to load-driven processes (Fig. 15c).

Over the NNW-oriented base-salt horst, salt and overburden translation across its steep, landward-dipping edge resulted in similar style of salt tectonics to that characterising the updip edge of Domain II (Fig. 7-8 and 15a). However, as the horst was of lower amplitude and the adjacent base-salt flat was narrower in Domain VI, extension-driven widening of pre-existing walls was relatively minor and no passive diapirs formed (Figs. 7 and 15). As a result, 4-6 km wide reactive walls developed over the horst in association with an ramp-syncline basin on their downdip flank (walls 13 and 14, RSB 7, fig. 15a). Further basinward, a new ramp-syncline basin formed over the basinward-dipping base-salt ramp bounding the downdip edge of a horst (RSB 6, fig. 15a). An associated fold-belt also formed as the system translated and decelerated over a contractional hinge present at the base of the ramp (Fig. 15a) (c.f. Dooley et al., 2016) (cf. Domain V; figs. 13-14a). This structural pattern is remarkably similar to physical and numerical models of translation over a pre-salt horst (Fig. 1d) (Dooley et al., 2016; Pichel et al., 2018; 2019b). The lack of closely-spaced pre-salt ramps meant that bulk shortening was less in Domain VI than in Domain V as indicated by the lack of highly squeezed salt structures (Fig. 3 and 15a).

Despite being subjected to c. 30 km of basinward translation (Pichel et al., 2018), base-salt relief had a reduced influence on salt tectonics in the north of Domain VI, away of the NNW extension of the Tupi Sub-High. As a result, salt-tectonics in the north of Domain VI was primarily driven by load-driven subsidence and passive diapirism with secondary, minor effects of salt flux variations over base-salt relief; both of which contributing to the observed polygonal pattern in the area (Figs. 5 and 15).

6. Discussion

6.1. Triggers, drivers and kinematics of salt-related deformation

The main phase of salt-related deformation in the SPP occurred during the Late Cretaceous to mid-Paleocene as the minibasin strata of this age display the most prominent thickness variations and intra-formational unconformities (Gamboa et al., 2008; Davison et al., 2012; Fiduk and Rowan, 2012; Guerra and Underhill, 2012; Jackson et al., 2015a) (Figs. 6-15). However, thickness changes in Albian strata document an earlier, albeit local phase of salt flow and related deformation (Fig. 4) (see also Davison et al., 2012; Quirk et al., 2012). Eocene-Neogene diapir fall (i.e. roof collapse facilitated by supra-diapir normal faults associated with salt 'horns'; figs. 7, 9 and 12), salt dissolution (Rodriguez et al., 2018), and local active rise by regional shortening of narrow walls (fig. 7a and 9a) are also observed. Their effects are however relatively minor compared to the preceding two phases of deformation. Here, we discuss the triggers, drivers and kinematics of the main phases of salt-related deformation in the SPP.

6.1.1. Early Deformation

Evidence for Aptian (i.e. syn-salt) related deformation in the SPP has been subject of intense debate (Gamboa et al., 2008; Davison et al., 2012; Quirk et al., 2012; Jackson et al., 2015a,b). This debate principally revolves around weather intra-salt thickness variations record syn-depositional deformation (Davison et al., 2012), or whether these reflect post-depositional flow controlled by strain partitioning across multiple intra-salt detachments (Albertz and Ings, 2012; Cartwright et al. 2012; Fiduk and Rowan, 2012; Dooley et al., 2015; Jackson et al., 2015b). Although not the focus of this study, we argue that minor syn-salt deformation may have occurred, but that most intra-salt thickness variations and complex internal structures record later deformation (i.e. Late Cretaceous-Paleocene) (Fiduk and Rowan, 2012; Jackson et al., 2015b, Dooley et al., 2015).

Albian deformation occurs predominantly in the north, in Domains IV and VI (Figs. 7 and 9a), and locally in Domains I-III (Fig. 4). Although interpretation of the deeper Albian structures is complicated by subsequent Late-Cretaceous-Paleocene deformation, Albian rise of NNE-to-NE-oriented salt bodies can be attributed to kinematically-linked inflation and/or contraction. This relatively minor contraction likely balanced at least some of the SE-directed extension that has been documented further updip, north-westward of the Albian Gap (c.f. Guerra and Underhill, 2012; Quirk et al., 2012; Davison et al., 2012). The origin of the WNW-NW-oriented Albian salt structures, however, and thus the polygonal framework locally developed on the SPP remains unclear. Some authors suggest it is related to S-SW-directed shortening due to an Eocene switch in sediment input (Guerra and Underhill, 2012), or Cretaceous convergent gliding driven by the concave-into-the-basin shape of the margin (Cobbold et al., 1995) (Fig. 1b and 16a). We dismiss the former interpretation given this invokes an Eocene age for the WNW-NW-oriented structures, when the majority of structures are clearly significantly older (i.e. Albian-early Paleocene; fig. 12d). The latter interpretation, although plausible, *cannot* explain why: (i) the WNW-NW-oriented structures developed only in the north of the study-area (Figs. 4-5); or (ii) the WNW-NW-oriented structures are associated with coeval (e.g. Late Cretaceous) reactive diapirs (Figs. 12 and 15).

Given that the area characterised by the greatest amount of Albian deformation and defined by the related polygonal pattern occurs at the edge of the dataset (Domains IV and VI), along the N and NE margins of the Tupi High, the triggers (and drivers) for this phase of deformation and related structural style may lie outside of our study-area. We therefore integrate structural maps presented by Guerra and Underhill (2012) to understand the origin of this somewhat enigmatic, WNW-trending suite of Albian salt walls. These maps, which cover an area immediate to the NW of our study-area, reveal a suite of E-to-ESE-oriented, low-relief salt rollers located in the immediate footwalls of salt-detached listric normal faults (Guerra and Underhill, 2012). These faults and rollers pass downdip, just to the north of our study area, into a series of WNW-, W-E and ENE-oriented structures contained within larger minibasins surrounded by variably-oriented salt walls (Fig. 16c). This structural pattern is markedly similar to what we observe in Domains IV and VI, where E-W- and NW-SE-oriented Albian contractional anticlines occur within larger minibasins (Figs. 4 and 12d), suggesting both formed in response to S- to SW-directed Albian shortening (Fig. 16d). Their predominance to the north of our study-area, coupled with their range of orientations (i.e. NW to ENE) and position relative to the Tupi Sub-High, suggest these folds developed in response to the obstruction of otherwise freely southwards-translating system and divergent flow around the major pre-salt structure. Similar features are observed in the physical models of Dooley et al.

(2018) (Fig. 11). Late Cretaceous WNW-oriented reactive diapirs overlie the Tupi High (Fig. 16d, Jackson et al., 2015a, their fig. 7a), indicating that early contractional structures were reactivated by extension as they moved over the pre-salt high. Similar deformation patterns occurred in Domains II and VI (figs. 7-8 and 15a-b), and are observed in physical (Dooley et al., 2016; 2018) and numerical models (Pichel et al., 2019b).

We thus broadly concur with Cobbold et al. (1995) that the polygonal arrangement of salt structures on the north of the study-area (domains IV and VI) is caused by bulk south- and south-eastward translation of salt and overburden driven by the concave-into-the-basin shape of the margin north of the study-area (Fig. 16a). However, key to the development of such variable structural trends is impingement of salt and overburden onto base-salt relief associated with the Tupi High and its NNW-oriented branch (Fig. 16b-d).

6.1.2. Late Cretaceous-Paleocene

The timing and origin of the main phase of salt-related deformation on the SPP are controversial (see section 1). The distribution, orientation and geometry of age-equivalent, salt-detached fold-belts in Domains I, V and VI are considered unequivocal evidence of Late Cretaceous-to-Paleocene shortening (Quirk et al., 2012; Guerra and Underhill, 2012; Fiduk and Rowan, 2012; Jackson et al., 2015b). However, these fold-belts are separated by relatively wide areas characterised by diapirs and minibasins that largely formed in response to translation, extension, and/or differential loading (domains II-IV; Figs. 7-12). We argue this observation shows shortening was not a widespread phenomenon as suggested by some workers (e.g. Quirk et al., 2012; Guerra and Underhill, 2012; Fiduk and Rowan 2012;

Alves et al., 2017), being instead focused and locally very intense updip of and above landward-dipping base-salt ramps and downdip of basinward-dipping ramps (Figs. 5-14).

Reactive, active and passive styles of diapirism are almost equally common across the SPP (Figs. 6-14). Over pre-salt highs (Sugar Loaf and Tupi), deformation is dominated by extension and reactive diapir rise or passive diapirism, following a brief, earlier phase of contraction (Fig. 7, 8, 13 and 15). Deformation at the edge of base-salt structures is characterized by map-view rotations and shearing due to map-view variations in velocity (i.e. salt flowing faster away of base-salt highs, cf. Dooley et al., 2018) and divergent flow around base-salt structures (Figs. 9-11 and 14b). Away from these areas, deformation is dominated by differential sedimentary loading and passive diapirism (Fig. 12). These observations, coupled with the existence of multiple ramp-syncline basins (Figs. 7, 9, 13 and 15) (Pichel et al., 2018) and the predominance of linear salt features parallel to the nearby base-salt relief (Figs. 3-5), indicate that the bulk of deformation in the SPP was driven by translation and associated salt flux variations across base-salt relief (Figs. 8, 10 and 14).

6.1.3. Salt Flow patterns

Salt and overburden translation, and the associated flux mismatches due to base-salt relief, are driven primarily by and associated with viscous shear drag (i.e. Couette flow, c.f. Weijermars et al., 1993; 2014; Rowan et al., 2004) within the salt (Fig. 17a) (Dooley et al., 2016; Pichel et al., 2018). In this case, salt streamlines (c.f. Dooley et al., 2016) can converge over base-salt landward-dipping ramps and diverge over basinward-dipping ramps producing, respectively, thickening and thinning of the flow section (Fig. 17a). Regions of thin and thick salt are more and less resistant, respectively, to flow, resulting in faster salt and overburden movement where salt is thicker and slower movement where salt is thinner. This ultimately produces zones of inflation and contraction at the updip edge of pre-salt highs, and zones of subsidence (monoclines), bound by hinges of updip extension and downdip contraction, above and immediately downdip of pre-salt highs (Fig. 17a) (Dooley et al., 2016) (Figs. 6-15).

This is, nonetheless, an idealized flow profile; i.e. in nature, salt flow is typically more complex in space and time due to intra-salt lithological and thus rheological heterogeneity (Weijermars et al. 2014; Jackson and Hudec, 2017) (Fig. 17b-c). In the case of a thick, mechanically layered salt, such as that present in the SPP, flow is expected to be complex due to intra-salt rheological variability and mechanical layering (c.f. Cartwright et al., 2012; Jackson et al., 2015b). The salt in the SPP is notably rich in bittern-salts, which comprise 15-35% of the most reflective intra-salt intervals (Rodriguez et al., 2018). These bittern salts are up to 10^6 times less viscous and flow 10^{2-5} times faster than halite (Van Keken et al., 1993; Jackson and Hudec, 2017); these units thus represent highly-mobile intra-salt detachments, which permit strong (vertical) flow partitioning.

Such partitioning is observed in physical models (Figs. 16b-c). During the early stage of deformation, when the supra-salt roof is of negligible thickness, first-order salt flow is driven by viscous shearing of the whole salt column following a typical Couette flow profile (Fig. 17b). Second-order flow within each discrete mobile interval (black) separated by more competent layers (coloured layers) is however more complex, varying from a typical Poiseuille flow profile (c.f. Rowan et al., 2004) at the lowermost level to hybrid, albeit Couette-dominated flow upward (Fig. 17b). This is seen in the

SPP, where the entire salt section has been sheared basinward, deforming primarily by Couette-flow as salt and overburden translated downdip, with the lowermost, halite-richest and thus more mobile level (A1; Jackson et al., 2015b; Rodriguez et al., 2018) being preferentially expelled basinward onto diapirs (Fig. 6-15). During the later stages of deformation, as the overburden gradually thickens and becomes more resistant to horizontal translation, flow becomes more hybrid; i.e. discrete salt intervals following a Poiseuille-flow pattern, although the first-order flow remains predominantly Couette (Fig. 17c).

6.2. Implications for the origin of the Albian Gap

The enigmatic Albian Gap corresponds to a c. 60 km wide structure in which the Albian (and underlying salt) section is largely absent, and Upper Cretaceous-Paleocene strata directly overlies (and is welded to) the pre-salt succession (Fig. 2) (Demercian et al., 1993; Szatmari et al., 1996; Jackson et al., 2015a). The controversy regarding its origin revolves around two end-member models, an extension-driven (Demercian et al., 1993; Mohriak et al., 1995; Quirk et al., 2012; Fiduk and Rowan 2012; Guerra and Underhill, 2012; Alves et al., 2017), and an expulsion-driven model (Ge et al., 1997; Gemmer et al., 2004; Jackson et al., 2015a,b). The former argues that the Albian Gap was formed by Late Cretaceous-Paleocene extension along a large (up to 60 km of heave), landward-dipping listric normal fault (i.e. the Cabo Frio Fault; CFF). The latter suggests the Albian Gap already existed by the end of Albian as an equally impressive, 60 km wide salt wall, and that Late Cretaceous-Paleocene expulsion by a prograding clastic wedge produced the basinward-dipping rollover and drove salt inflation in the SPP. Whereas the extension-driven model invokes bulk shortening further downdip in the SPP, the expulsion-model invokes bulk inflation without shortening.

Pichel et al. (2018) demonstrate that salt and its overburden on the SPP, immediately downdip of the Albian Gap, underwent 28-32 (±2) km of bulk SE-directed post-Albian translation, a process not identified in previous studies or incorporated in the two end-member models described above. Translation was primarily recorded by ramp-syncline basins (Pichel et al., 2018) and the variable style of deformation with localized extension and shortening as salt and overburden moved basinward across base-salt ramps. In kinematically-linked gravity-driven systems an intermediate zone of translation links domains of updip extension, and downdip contraction and/or salt advance (Rowan et al., 2004; Hudec and Jackson 2007; Jackson et al., 2015a, Peel 2014b, Allen et al., 2016). Thus, the c. 30 km of Late Cretaceous-Paleocene basinward translation on the SPP should be balanced by similar amounts of either coeval updip extension, and downdip contraction and/or salt advance (Rowan et al., 2004; Peel 2014b; Jackson et al., 2015a). This may consequently help us understand the regional kinematics of the Central Santos Basin and, specifically, the origin of the enigmatic Albian Gap.

A c. 30 km wide salt nappe is developed along most of the downdip edge of the Santos Basin (Fig. 1c-d) (Davison et al., 2012; Quirk et al 2012). This nappe is estimated to have formed during the Late Cretaceous (Davison et al., 2012), and is thus of approximately the same age as the main period of translation we document here and in Pichel et al. (2018). Furthermore, the magnitude of nappe advance broadly balances our estimate of the bulk downslope translation (c. 30 km) on the SPP (see also Pichel et al., 2018).

Updip of the SPP, extension is well-documented by an array of salt-detached normal faults and salt rollers that formed during the Albian (Guerra and Underhill, 2012; Davison et al., 2012; Quirk et al., 2012). These are thus older than the ramp-syncline basins we document on the SPP, implying that the recorded 30 km of translation must have been accommodated elsewhere, possibly in the Albian Gap, which is located between this zone of Albian extension and the SPP.

Based on: (i) our recognition that Late Cretaceous-Paleocene ramp-syncline basins record c. 30 km of SE-directed translation; (ii) the multiphase style of complex diapirism present on the SPP; and (iii) the geometry of post-Albian strata filling the it (c.f. Jackson et al., 2015a), we propose a new model for the origin of the enigmatic Albian Gap (Fig. 18). In our model Albian extension led to the development of c. 30 km wide, reactive salt wall that reached the Albian paleo-seafloor (Fig. 18a-b). This structure is similar in origin to the one proposed by Jackson et al. (2015) but is half as wide. During the Late Cretaceous-Paleocene this wall was widened by an additional 30 km and likely fell in response to thin-skinned extension, whilst simultaneously being loaded by clastic sediment prograding seaward from the continent (Fig. 17b-c). This resulted in the seaward expulsion of salt onto the SPP, development of large, landward-dipping, listric normal fault (CFF), and formation of the presently c. 60 km wide Albian Gap. Strata filling the Albian Gap is thus a hybrid expulsion-extensional rollover (Fig. 18c). In summary, our analysis suggests the Albian Gap formed by a combination of processes; at least 30km of Late Cretaceous-Paleocene extension must have occurred in order to balance the downdip translation in the SPP (Fig. 18c). The additional 30 km of the gap may be explained by earlier, Albian extension (Fig. 18b) and/or as an original depositional gap over a very wide salt wall.

7. Conclusions

The geometries, kinematics and distribution of salt structures and minibasins on the SPP, Santos Basin, Brazil and their relationship with base-salt structures confirms that salt tectonics in the São Paulo Plateau was controlled by non-uniform basinward translation of thick, layered salt over variable base-salt relief. Viscous salt drag generated salt flux variations due to initial salt thickness contrasts across base-salt structures. Variations in the rate of basinward salt flow resulted in variable and localized contractional and extensional deformation, multiphase diapirism, and the development of ramp-syncline basins. Salt structures and minibasins away from the main base-salt structures are geometrically and kinematically simpler, with their growth dominated by load-driven processes. At the edge of or along pre-salt highs, deformation was characterized by plan-view differential flow, rotation and shearing.

Ramp-syncline basins provide a record of c. 30 km of horizontal translation of salt and overburden across the SPP during the Late Cretaceous-Paleocene. This can be extrapolated to neighbouring structural domains and therefore can help constrain the origin and kinematics of the controversial updip Albian Gap. We propose that the 50-60 km wide gap formed by a combination of lateral extension and salt expulsion, with c. 20-30 km of Albian extension followed by additional c. 30 km of Late Cretaceous-Paleocene extension that balances the 30 km of coeval translation downdip in the SPP. Late Cretaceous-Paleocene extension occurred in tandem with expulsion of an early-formed 20-30 km wide salt wall; this generated the large-scale rollover structure presently overlying the Albian Gap. The concepts presented here can improve the comprehension of complex salt-related deformation through time and space in various salt basins affected by thin-skinned gravity-driven deformation and translation above a dipping, irregular salt detachment.

Acknowledgements

The authors wish to thank Mike Hudec, Oliver Duffy, Mads Huuse, Mark Rowan and Gillian Apps for the fruitful discussions and constructive criticism. We also thank Ian Davison and Maria Roma for their constructive reviews, and Atle Rotevatn for excellent editorial handling. We thank CGG for providing access to the high-quality 3D seismic dataset used in this study and WesternGeco for the PSDM 2D transects. The main author would also like to thank the Science without Borders program and CNPq, Brazil for sponsoring his PhD research. Schlumberger is also acknowledged for provision of Petrel software.

References

Albertz, M., & Ings, S. J., 2012. Some consequences of mechanical stratification in basin-scale numerical models of passive-margin salt tectonics. Geological Society, London, Special Publications, 363(1), 303-330.

Allen, H., Jackson, C. A. L., Fraser, A. J., 2016. Gravity-driven deformation of a youthful saline giant: the interplay between gliding and spreading in the Messinian basins of the Eastern Mediterranean. Petroleum Geoscience, 22(4), 340-356.

Alves, T. M., Fetter, M., Lima, C., Cartwright, J. A., Cosgrove, J., Gangá, A, Strugale, M., 2017. An incomplete correlation between pre-salt topography, top reservoir erosion, and salt deformation in deep-water Santos Basin (SE Brazil). Marine and Petroleum Geology, 79, 300-320.

Beloussov, V. V., 1959. Types of folding and their origin. International Geology Review, 1(2), 1-21.

Brown, A. R., 2011. Interpretation of three-dimensional seismic data. Society of Exploration Geophysicists and American Association of Petroleum Geologists.

Brun, J. P., Fort, X., 2011. Salt tectonics at passive margins: Geology versus models. Marine and Petroleum Geology, 28(6), 1123-1145

Cartwright, J., Jackson, M., Dooley, T., Higgins, S., 2012. Strain partitioning in gravity-driven shortening of a thick, multilayered evaporite sequence. Geological Society, London, Special Publications, 363(1), 449-470.

Contreras, J., Zühlke, R., Bowman, S., Bechstädt, T., 2010. Seismic stratigraphy and subsidence analysis of the southern Brazilian margin (Campos, Santos and Pelotas basins). Marine and Petroleum Geology, 27(9), 1952-1980.

Cobbold, P. R., Szatmari, P., Demercian, L. S., Coelho, D., Rossello, E. A. (1995). Seismic and experimental evidence for thin-skinned horizontal shortening by convergent radial gliding on evaporites, deep-water Santos Basin, Brazil, *in*: Jackson, M. P. A., Roberts, D. G., Snelson, S. (eds) Salt tectonics: a global perspective. AAPG Memoir 65, 305-321.

Demercian, S., Szatmari, P., Cobbold, P. R., 1993. Style and pattern of salt diapirs due to thin-skinned gravitational gliding, Campos and Santos basins, offshore Brazil. Tectonophysics, 228(3-4), 393-433.

Davison, I., Anderson, L., Nuttall, P., 2012. Salt deposition, loading and gravity drainage in the Campos and Santos salt basins. Geological Society of London Special Publications, 363(1), 159-174.

Dooley, T. P., Jackson, M. P., Jackson, C. A. L., Hudec, M. R., Rodriguez, C. R., 2015. Enigmatic structures within salt walls of the Santos Basin—Part 2: Mechanical explanation from physical modelling. Journal of Structural Geology, 75, 163-187.

Dooley, T. P., Hudec, M. R., Carruthers, D., Jackson, M. P., Luo, G., 2016. The effects of base-salt relief on salt flow and suprasalt deformation patterns—Part 1: Flow across simple steps in the base of salt. Interpretation, 5(1), SD1-SD23.

Dooley, T. P., Hudec, M. R., 2016. The effects of base-salt relief on salt flow and suprasalt deformation patterns—Part 2: Application to the eastern Gulf of Mexico. Interpretation, 5(1), SD25-SD38.

Dooley, T. P., Hudec, M. R., Pichel, L. M., Jackson, M. P., 2018. The impact of base-salt relief on salt flow and suprasalt deformation patterns at the autochthonous, paraautochthonous and allochthonous level: insights from physical models. Geological Society, London, Special Publications, 476, SP476-13.

Fiduk, J. C., Rowan, M. G., 2012. Analysis of folding and deformation within layered evaporites in Blocks BM-S-8 &-9, Santos Basin, Brazil. Geological Society, London, Special Publications, 363(1), 471-487.

Gamboa, L.A.P., Machado, M.A.P., Silveira, D.P., Freitas, J.T.R., Silva, S.R.P., 2008. Evaporitos estratificados no Atlântico Sul: interpretação sísmica e controle tectono-estratigráfico na Bacia de Santos. In: W. Mohriak, P. Szatmari & S. M. C. Anjos (Org.), Sal: Geologia e Tectônica. Editora Beca, São Paulo, 2ed., p. 343-361.

Ge, H., Jackson, M. P., Vendeville, B. C., 1997. Kinematics and dynamics of salt tectonics driven by progradation. AAPG bulletin, 81(3), 398-423.

Gemmer, L., Ings, S.J., Medvedev, S. Beaumont, C., 2004. Salt tectonics driven by differential sediment loading: stability analysis and finite-element experiments. Basin Research, 16(2), 199-218.

Guerra, M. C., Underhill, J. R., 2012. Role of halokinesis in controlling structural styles and sediment dispersal in the Santos Basin, offshore Brazil. Geological Society, London, Special Publications, 363(1), 175-206.

Hudec, M. R., Jackson, M. P. A., 2004. Regional restoration across the Kwanza Basin, Angola: Salt tectonics triggered by repeated uplift of a metastable passive margin. AAPG bulletin, 88(7), 971-990.

Hudec, M. R., Jackson, M. P., 2006. Advance of allochthonous salt sheets in passive margins and orogens. AAPG bulletin, 90(10), 1535-1564.

Hudec, M. R., Jackson, M. P., 2007. Terra infirma: Understanding salt tectonics. Earth-Science Reviews, 82(1), 1-28.

Hudec, M. R., Jackson, M. P., Schultz-Ela, D. D. 2009. The paradox of minibasin subsidence into salt: Clues to the evolution of crustal basins. Geological Society of America Bulletin, 121(1-2), 201-221.

Jackson, M. P. A., Hudec, M. R., Fraenkl, R., Sikkema, W., Binga, L., Da Silva, J. 2001. Minibasins translating down a basement ramp in the deepwater monocline province of the Kwanza Basin, Angola [abs.]. In: American Association of Petroleum Geologists Annual Meeting Official Program, 10, A99.

Jackson, M. P., Hudec, M. R., 2005. Stratigraphic record of translation down ramps in a passive-margin salt detachment. Journal of Structural Geology, 27(5), 889-911.

Jackson, M.P., Hudec, M.R., 2017. Salt Tectonics: Principles and Practice. Cambridge University Press.

Jackson, C. A., Jackson, M. P., Hudec, M. R., Rodriguez, C., 2014a. Internal structure, kinematics, and growth of a salt wall: Insights from 3-D seismic data. Geology, 42(4), 307-310.

Jackson, C. A. L., Rodriguez, C. R., Rotevatn, A., Bell, R. E., 2014b. Geological and geophysical expression of a primary salt weld: An example from the Santos Basin, Brazil. Interpretation, 2(4), SM77-SM89.

Jackson, C. A. L., Jackson, M. P., Hudec, M. R., 2015a. Understanding the kinematics of salt-bearing passive margins: A critical test of competing hypotheses for the origin of the Albian Gap, Santos Basin, offshore Brazil. Geological Society of America Bulletin, 127(11-12), 1730-1751.

Jackson, C. A. L., Jackson, M. P., Hudec, M. R., Rodriguez, C. R. 2015b. Enigmatic structures within salt walls of the Santos Basin—Part 1: Geometry and kinematics from 3D seismic reflection and well data. Journal of Structural Geology, 75, 135-162.

Karner, G. D., Gambôa, L. A. P., 2007. Timing and origin of the South Atlantic pre-salt sag basins and their capping evaporites. Geological Society, London, Special Publications, 285(1), 15-35.

Krézsek, C., Adam, J. and Grujic, D., 2007. Mechanics of fault and expulsion rollover systems developed on passive margins detached on salt: insights from analogue modelling and optical strain monitoring. Geological Society, London, Special Publications, 292(1), pp.103-121.

Marton, G., Tari, G. Lehmann, C., 1998. Evolution of salt-related structures and their impact on the post-salt petroleum systems of the Lower Congo Basin, offshore

Angola. In: American Association of Petroleum Geologists International Conference and Exhibition, Rio de Janeiro. Extended Abstracts Volume, 834–834.

Meisling, K. E., Cobbold, P. R., Mount, V. S., 2001. Segmentation of an obliquely rifted margin, Campos and Santos basins, southeastern Brazil. AAPG bulletin, 85(11), 1903-1924.

Modica, C. J., Brush, E. R., 2004. Postrift sequence stratigraphy, paleogeography, and fill history of the deep-water Santos Basin, offshore southeast Brazil. AAPG bulletin, 88(7), 923-945.

Mohriak, W.U., Macedo, J.M., Castellani, R.T., Rangel, H.D., Barros, A.Z.N., Latgé, M.A.L., Mizusaki, A.M.P., Szatmari, P., Demercian, L.S., Rizzo, J.G. Aires, J.R. (1995). Salt tectonics and structural styles in the deep-water province of the Cabo Frio region, Rio de Janeiro, Brazil, *in*: Jackson, M. P. A., Roberts, D. G., Snelson, S. (eds) Salt tectonics: a global perspective. AAPG Memoir 65, 273-304.

Mohriak, W., Nemčok, M., Enciso, G., 2008. South Atlantic divergent margin evolution: rift-border uplift and salt tectonics in the basins of SE Brazil. Geological Society, London, Special Publications, 294(1), 365-398.

Mohriak, W.U., Szatmari, P., Anjos, S.M.C., 2009. Sal: Geologia e Tectônica. Editora Beca, São Paulo,450 pp

Mohriak, W. U., Szatmari, P., Anjos, S., 2012. Salt: geology and tectonics of selected Brazilian basins in their global context. Geological Society, London, Special Publications, 363(1), 131-158.

Peel, F., Jackson, M.P. Ormerod, D., 1998 Influence of Major Steps in the Base of Salt on the Structural Style of Overlying Thin-skinned Structures in Deep Water

Angola, American Association of Petroleum Geologists International Conference and Exhibition, Rio de Janeiro, Brazil, November, Extended Abstracts Volume, pp. 366-367.

Peel, F. J., 2014b. The engines of gravity-driven movement on passive margins: Quantifying the relative contribution of spreading vs. gravity sliding mechanisms. Tectonophysics, 633, 126-142.

Pichel, L.M., Peel, F., Jackson, C.A.-L., Huuse, M., 2018, Geometry and kinematics of salt-detached ramp syncline basins, Journal of Structural Geology, 115, 208-230. in press, doi: 10.1016/ j.jsg.2018.07.016.

Pichel, L. M., Finch, E., Gawthorpe, R., 2018b. Impacts of Pre-salt Rift Topography on Salt Tectonics

Quirk, D. G., Schødt, N., Lassen, B., Ings, S. J., Hsu, D., Hirsch, K. K., Von Nicolai, C., 2012. Salt tectonics on passive margins: examples from Santos, Campos and Kwanza basins. Geological Society, London, Special Publications, 363(1), 207-244.

Rodriguez, C. R., Jackson, C. L., Rotevatn, A., Bell, R. E., Francis, M., 2018. Dual tectonic-climatic controls on salt giant deposition in the Santos Basin, offshore Brazil. Geosphere, 14(1), 215-242.

Rowan, M. G., Weimer, P., 1998. Salt-sediment interaction, northern Green Canyon and Ewing bank (offshore Louisiana), northern Gulf of Mexico. AAPG bulletin, 82(5), 1055-1082.

Rowan, M. G., Jackson, M. P., Trudgill, B. D., 1999. Salt-related fault families and fault welds in the northern Gulf of Mexico. AAPG bulletin, 83(9), 1454-1484.

Rowan, M. G., Trudgill, B. D., Carl Fiduk, J., 2000. Deep-Water, Salt-Cored Fold-belts: Lessons from the Mississippi Fan and Perdido Fold-belts, Northern Gulf of Mexico. Atlantic rifts and continental margins, 173-191.

Rowan, M. G., Peel, F. J., & Vendeville, B. C. (2004). Gravity-driven fold-belts on passive margins.

Rowan, M. G., Giles, K. A., Hearon IV, T. E., Fiduk, J. C., 2016. Megaflaps adjacent to salt diapirs. AAPG Bulletin, 100(11), 1723-1747.

Szatmari, P. M. C. M., Guerra, M. C. M., & Pequeno, M. A. (1996). Genesis of large counter-regional normal fault by flow of Cretaceous salt in the South Atlantic Santos Basin, Brazil. Geological Society, London, Special Publications, 100(1), 259-264.

Van Keken, P.E., Spiers, C.J., Van den Berg, A.P. and Muyzert, E.J., 1993. The effective viscosity of rocksalt: implementation of steady-state creep laws in numerical models of salt diapirism. Tectonophysics, 225(4), pp.457-476.

Vendeville, B. C., Jackson, M. P. A., 1992a. The rise of diapirs during thin-skinned extension. Marine and Petroleum Geology, 9(4), 331-354.

Weijermars, R., Jackson, M.T., Vendeville, B., 1993. Rheological and tectonic modeling of salt provinces. Tectonophysics 217 (1–2), 143–174.

Weijermars, R., Jackson, M. P., Dooley, T. (2014). Predicting the depth of viscous stress peaks in moving salt sheets: Conceptual framework and implications for drilling Viscous Stress Peaks in Moving Salt Sheets. AAPG bulletin, 98(5), 911-945.

Figure Captions

Figure 1: (a) Schematic cross-sections demonstrating classical distribution and style of gravity-driven salt tectonics along continental margins, with an updip extensional domain passing downdip to an intermediate and undeformed translational province and a downdip

shortening domain (adapted from Davison et al., 2012 and Jackson et al., 2015a). (b) Schematic cross-sections based on physical models showing the effects of base-salt relief and thickness variations on salt flow and overburden deformation (after Dooley et al., 2016). (c) Location map of the study-area, the São Paulo Plateau, Central Santos Basin Brazil with the main salt-related structural provinces indicated. Our 3D seismic survey is highlighted in red and other previous studies location in polygons with different colours. Black line is the location of the geoseismic section presented in (d) showing the main structural elements of the study-area, with the Albian gap and the associated Cabo-Frio Fault (CFF) updip, passing downdip to a zone of thickened salt over complex and prominent base-salt topography of the Tupi Sub-High, and further downdip to a frontal salt nappe.

Figure 2: Uninterpreted and interpreted regional PSDM (pre-stack depth-migrated) line showing the main salt-related structural elements of the Central Santos Basin: an updip extensional domain, a c. 60km of Albian Gap, The São Paulo Plateau (SPP) and a deep-salt basin domain characterized by high-amplitude, squeezed diapirs and allochthonous salt sheets. The base-salt geometry is characterized by a series of landward- and basinward-dipping base-salt ramps with up to 2 km of structural relief associated to rift normal faults that generate base-salt drape folds and/or small offsets (location in fig. 1, 3 and 4).

Figure 3: Static-corrected base-salt (BoS) structure map illustrating the main base-salt highs and associated ramps in (a), and overlay of different structural domains of the SPP and location of sections presented in this study in (b). LW and BW refer to landward- and basinward-dipping base-salt ramps, respectively. The black polygon in (a) corresponds to the location of the depth base-salt structure map adapted from Alves et al. (2017) shown in (c) for comparison.

Figure 4: (a) TWT top-salt structure map showing the framework of salt walls and minibasins oriented predominantly NNE orientation but becoming more complex and polygonal north-eastwards. (b) Simplified structural map outlining key structures and structural domains of the SPP and coloured accordingly to the timing of onset of growth, with blue indication earlier, Albian growth, and pink, Late Cretaceous. Seismic sections presented here in orange.

Figure 5: Overlay of salt structures over static-corrected base-salt (BoS) map illustrating the broadly sub-parallel orientation of salt and base-salt structures and location of salt walls and anticlines relative to base-salt relief.

Figure 6: (a-c) NW-SE oriented seismic lines showing a salt-cored fold-belt above a landward-dipping base-salt ramp and broadly thick salt on Domain I. The fold-belt present variable fold geometries but are predominantly cored by intra-salt shear zones (thick-black lines) and affected by outer-arc extension, with occasional reactive piercement on their core, which typically occurs where the base-salt becomes flat. Faults in black and pre-kinematic, tabular roof indicated by white ticks, which becomes progressively thicker landward showing the general younging direction of the fold-belt. White lines below base-salt indicate base-salt geometry estimated by subtracting the obvious velocity pull-ups (indicated) below thicker salt bodies. (d) SW-NE oriented seismic section over the salt walls and minibasins in the area with large salt evacuation at their centre due to a combination of extension and load-driven subsidence associated to ponding of mass-transport complexes (MTCs).

Figure 7: Seismic section of Domain II, with (a-b) WNW-ESE sections showing wide salt walls affected by intra-salt complex deformation and seaward-vergent shear zones and affected predominantly by inward-dipping and younging growth normal faults in their flanks and intercalated with RSBs and few salt-cored folds. The Albian interval is predominantly isopachous with only minor, local Albian growth of wall 3 in (a) and the bulk of supra-salt

thickness variation occurring from Late Cretaceous-Paleocene within RSBs. (c) Same section of (b) with a pink polygon representing the salt interval with its base-salt (BoS') static-corrected horizon showing the real base-salt geometry and the presence of a large landward-dipping ramp. (d) zoom of RSB 2a and (e) zoom of RSB 1b, with arrows indicating onlaps (yellow) and erosional truncations (red) within RSBs in (d) and (e). (f) Section showing Late Cretaceous-Paleocene reactive salt walls that form along-strike, at the edge of the large salt walls 2 and 3 intercalated with Late-Cretaceous-Paleocene gentle salt-cored folds.(g) Section showing a similar reactive salt wall nucleating on the core of salt-cored fold formed by earlier contraction as indicated by the intra-salt shear zone. See legend on fig.5.

Figure 8: Kinematic models showing evolution of salt walls of Domain II and landward-propagation of shortening and the fold-belt of Domain I by translation over a set of base-salt landward-dipping ramps over the Sugar Loaf High. In (a), model with initial salt relief due to an earlier Albian growth phase (Phase I) and, in (b), no earlier Albian growth (tabular Albian in green). As translation starts (Phase II) the system becomes temporarily pinned above the ramps and, due to initial thickness variations controlled by basal relief, the cross-sectional area of salt flowing onto the ramps is greater than the one flowing out; producing salt inflation and contraction. Continuous salt inflation and translation leads to progressive widening of the salt structure and development of RSBs over their basinward-flank above the base-salt flat where movement is faster; whereas their landward-flanks keep being uplifted and upturned. In the case of an earlier, Albian phase of growth (a), inflation results in piercement by active diapirism (Phase II), with eventual breakthrough and passive diapirism (phase III). In the case of no previous growth (b), inflation results in development of a salt-cored buckle fold (Phases II-III). During Phases III-IV, differential translation and continuous thickening allow the velocity to build-up and the salt structure to eventually leave the ramp while extending over the base-salt high. In the case of an earlier passive diapir (a), extension is mostly cryptic and results in wide passive salt walls; whereas in the case of salt anticlines (b), a reactive diapir nucleates at their crests. As translation continues, contraction propagates landward and new salt-cored buckle-folds form as salt flow keeps being buttressed against the landward-dipping ramps (Phase IV).Pre-folding tabular interval indicated by a red tick on buckle-fold.

Figure 9: (a-b) NW-SE sections illustrating salt wall 5, which forms above narrow base-salt horst block at the edge of the Sugar-Loaf and is characterized by complex intra-salt deformation with intra-salt shear zone indicating early inflation, followed by extension and passive growth. The large width of the wall suggests part of the extension is cryptic, being accommodated by widening. This wall is limited downdip by a thick minibasins showing two thin RSBs sections that formed by translation above both base-salt ramps delimiting the pre-salt high. Further downdip, wall 6 occurs over another base-salt high and is characterized by a narrow reactive salt wall formed above a salt-cored fold to the north, at the edge of the base-salt high (a); and a wide salt wall with stronger evidence of contraction (intra-salt shearing and buckle-folding on its basinward-flank).In (c), the same section from (b) with a pink polygon representing the salt interval with its base-salt (BoS') static-corrected horizon showing the real base-salt geometry and the presence of the base-salt horst beneath wall 5 and a landward-dipping ramp beneath wall 6. See legend on fig.5

Figure 10: (a) Complex base-salt geometries at the edge of the Sugar-Loaf High (extracted from base-salt map of figure 3) with ramps highlighted by grey polygons showing a NNE-oriented base-salt horst-branch passing downdip to a NE-oriented landward-dipping ramp and further downdip to an ENE relay zone. (b) Kinematic model showing distribution of salt walls from Domains II and III, with marked shearing and rotation where base-salt topography abruptly changes, especially at the edge of the Sugar Loaf High. Structures to the south (walls 2 and 3), over the Sugar Loaf High are oriented NNE, sub-parallel to the base-salt, curving progressively to the NE northwards (wall 5). Structures further downdip, landward and over the ENE-oriented relay zone (walls 4 and 6) are also oriented sub-parallel to the

ENE-NE structures, suggesting clockwise rotation and shearing relative to structures further south and/or landward. The wall over the NNE-oriented base-salt updip horst-branch (5) is sheared and rotated counter-clockwise as it reaches earlier a base-salt high, relative to its counterpart further south (wall 3), over the Sugar Loaf High. The RSB formed immediately downdip of this NNE high translates and rotates clockwise and the wall further downdip over the NE-oriented base-salt high is sheared clockwise as its northern edge is able to move faster while its southern part is being buttressed against the edge of the Sugar-Loaf; producing a sigmoidal plan-view geometry (wall 6).

Figure 11 (a-b): Physical models simulating gravity-driven salt-detached translation around three discontinuous pre-salt tilted blocks (SSH) and the effects of base-salt relief on salt flow with pre-salt blocks highlighted in white boxes (adapted from Dooley et al., 2018). (a) Overhead views showing rotation up to 67° at the edge of the pre-salt blocks. (b) Dip-parallel displacement (I and III) and Y motions (N-S movements, II and IV) of relative of same time-ramps of (a) showing divergent flow around the updip edges of pre-salt block and convergent flow around their downdip edges. For full model design and material details, see Dooley et al. (2016).

Figure 12: (a-b) NW-SE oriented seismic sections of Domain IV showing tall salt walls (7-9) and with abrupt flank upturns and thick, welded minibasins with abrupt cutoffs and onlaps against the walls and turtle or bowl geometries, and raised rims. These aspects indicate they formed primarily by load-driven subsidence and passive diapirism over a broadly flat base-salt topography. Walls further downdip (9-11) become more affected by normal faults, denoting progressively earlier effects of regional stresses, mainly associated with extension. (c) NW-SE narrow reactive salt walls formed at the south edge of Domain IV, near Domain III. (d) Wider NW-SE reactive salt wall further north, showing signs of earlier load-driven growth, a large turtle anticline formed above a set of Albian narrow and abrupt anticlines. See legend on fig.5

Figure 13: Dip-oriented seismic sections illustrating salt-related structural styles and associated RSBs over the Tupi High and smaller pre-salt tilted blocks further downdip in Domain V. (a-b) Regional sections showing contraction (buckle-folds) over the landward-dipping edge of the Tupi High, passing downdip to extended folds and reactive diapirs over the broadly flat base-salt segment downdip, subsidence and development of RSBs above the large basinward-dipping base salt and a contractional fold-thrust belt further downdip. (b) Same section with a salt polygon and the base-salt static-corrected horizon (BoS') showing the real base-salt geometry. (c) Close-up of updip salt-cored buckle folds formed by buttressing against the crest of the Tupi High, monoclinal geometry overlain by a RSB over the large base-salt basinward-dipping ramp and additional contraction immediately downdip of it, with stacking of intra-salt reverse shear zones, buckle-folding and thickening of the salt interval. (d) Section showing minor updip extension represented by reactive rise at the crest of an earlier contractional structure over the crest of the Tupi High, passing downdip to an open fold and RSB above its basinward-dipping ramp and further downdip to a zone of major contraction characterized by a fold-thrust belt associated with RSBs and squeezed diapirs, fold injection and thrust piercement due to renewed pulses of contraction as salt and overburden translated over series of closely-spaced smaller pre-salt highs. (e) Section showing similar features downdip of the Tupi High and along-strike variation of a squeezed diapir from (d) to back-thrust-piercement of salt (wall 12). (f) Section showing stacking of reverse basinward-vergent intra-salt shear zones and consequent thickening of the salt interval with active piercement and disruption of the fold-belt roof behind the large pre-salt high downdip of the largest Tupi High. See legend on fig.5

Figure 14: (a) Kinematic model showing the cross-sectional evolution of Domain V by translation over the Tupi High and closely-spaced pre-salt tilted blocks downdip. Translation over the gentle landward-dipping step of the Tupi results in partial pinning of the system against the crest of the Tupi High and development of a fold-belt updip. Translation over the

Tupi High basinward-dipping edge results in salt subsidence, development of RSBs above it and contraction further downdip as movement is buttressed by a series of smaller variably-dipping base-salt ramps, in which RSBs also form over their basinward-dipping side. Mild extension occurs at the crest of the Tupi High, resulting in minor faulting and unfolding of earlier folds formed updip. Extension is, however, overprinted by contraction as the system moves downdip over the set of smaller base-salt highs where renewed pulses of contraction resulting in fold-injection, squeezing and thrust piercement. (b) Map-view kinematic model illustrating radial flow around a smaller, broadly rectangular pre-salt high; which results in divergence around it and convergence and pinning behind it. This produces coalescence and thickening of salt-cored folds and development of NW-oriented walls behind the smaller pre-salt highs.

Figure 15: NW-SE sections of Domain VI: (a) Seismic section to the south, over the NNW-oriented branch of the Tupi High showing reactive salt walls over the base-salt horst passing to a salt-cored contractional fold-belt downdip of it, all being associated with Late Cretaceous-Paleocene RSBs. The largest walls show an earlier, Albian phase of growth, with significant thickness variations and top-Albian unconformities. (b) Same section with static-corrected base-salt (BoS') to illustrate the real base-salt geometry. (c) Section to the north, farther of the Tupi High, showing similar style of deformation with a broader reactive salt wall updip and a gentler fold-belt associated with RSBs further downdip, but with relatively stronger influence of load-driven processes as seen by intermediate nearly welded, broadly symmetric minibasins and a salt wall driven by halokinetic active diapirism. White dashes lines indicate regional associated with overburden normal faults. See legend on fig.5

Figure 16: (a) Location map adapted from Guerra and Underhill (2012) showing the bathymetry and curvature of the margin and the associated Cretaceous hinge line. Their study-area in black and ours in white polygons with their equivalent regional, 2D based top-salt structure map in (b); and combination of our top-salt structure map with their 3D-based top-salt structure map located immediately to the north of our study-area. In (d) a simplified diagram combining the two maps and showing the presence of W-E to NW-SE extensional ridges north of our study-area, passing southwards to contractional anticlines that diverge around the Tupi High, with few structures moving over the high and being reactivated as extensional, reactive salt walls.

Figure 17: Idealized viscous shear drag (i.e. Couette flow) model showing salt streamlines (black line) and flux variations across base-salt relief that resulted in the observed deformational style in the SPP. Salt inflation and contraction over base-salt landward-dipping ramps (horst updip edge) and subsidence with updip extension and downdip contraction over base-salt basinward-dipping ramps (horst downdip edge). (b)-(c) Physical models simulating salt-detached translation of a mechanically-layered salt with (a) negligible roof and (b) thick roof showing a first-order Couette flow profile and more variable second-order flow; both of which evolve through time and become more complex and affected by Poiseuille flow as the overburden thickens (adapted from Weijermars et al., 2014). Viscous silicone polymer simulating salt (black) alternates with frictional-plastic dry sand (thin, coloured layers, each 1 mm thick). Yellow parabolas represent originally vertical passive markers within the salt. For full model details, see Cartwright et al. (2012).

Figure 18: Kinematic model explaining the origin of the Albian Gap by 30 km of Albian extension producing an Albian reactive-passive diapir (a-b), and (c) additional 30 km of extension with coeval salt expulsion during the Late Cretaceous-Paleocene.

Appendix Figure: Table showing a zoom of the key, most distinctive types of structures associated with complex, multiphase deformation and salt flux variations observed in different domains in the study-area: (a) salt-cored buckle-folds; (b) collapsed folds; (a-b) transition from buckle-folds into collapsed folds over extensional hinge at the crest of the Tupi Sub-High; (c) reactive diapirs; (d) reactive diapirs nucleating onto salt-cored buckle-

folds; (e) passive diapirs; (f) squeezed diapirs; (g) fold-injection; (h) thrust-piercement; and (i) multiphase diapirs.

Figures

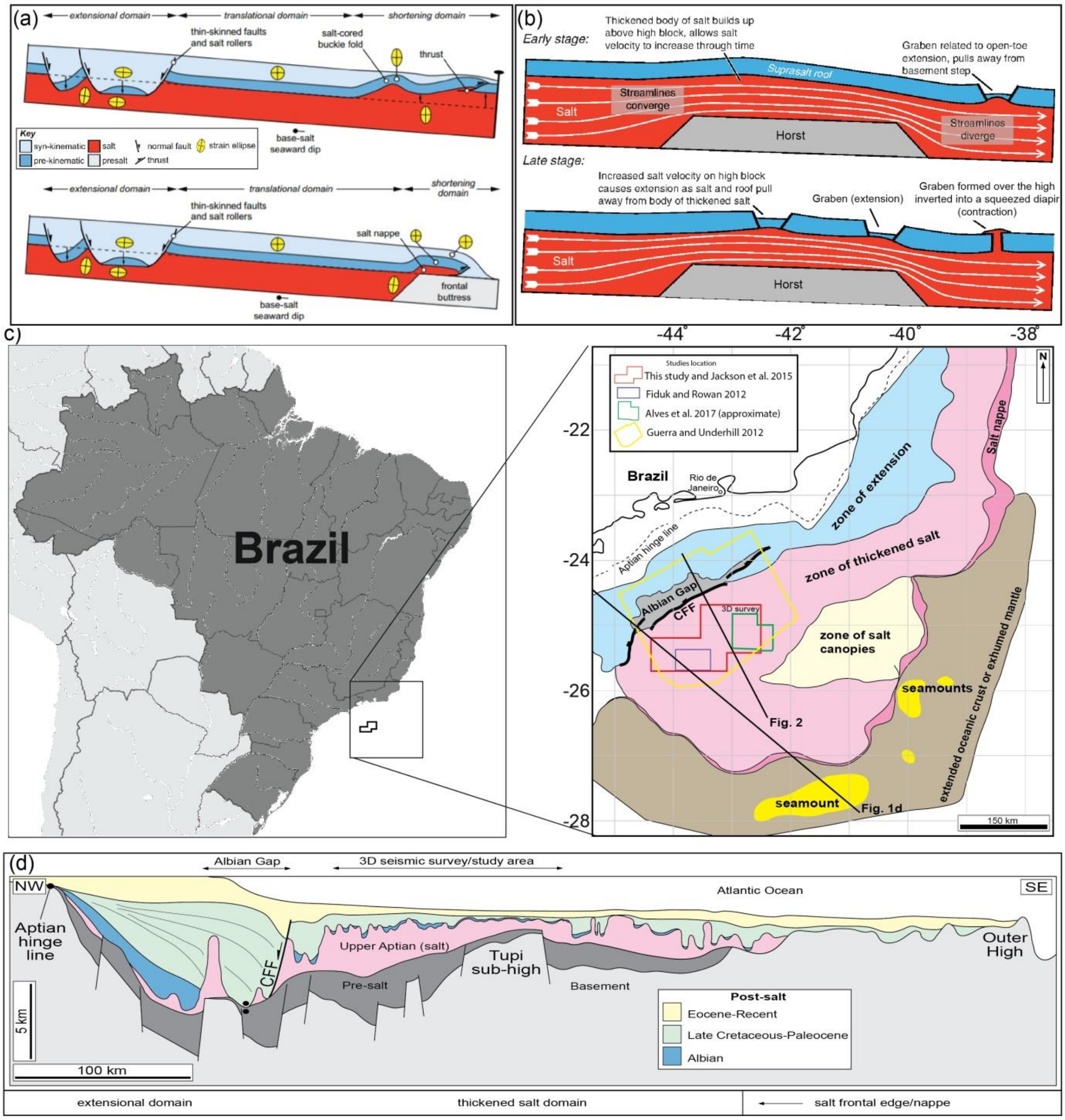

Figure 1

Figure 2: PSDM regional section (not displayed, awaiting finalizing permission)

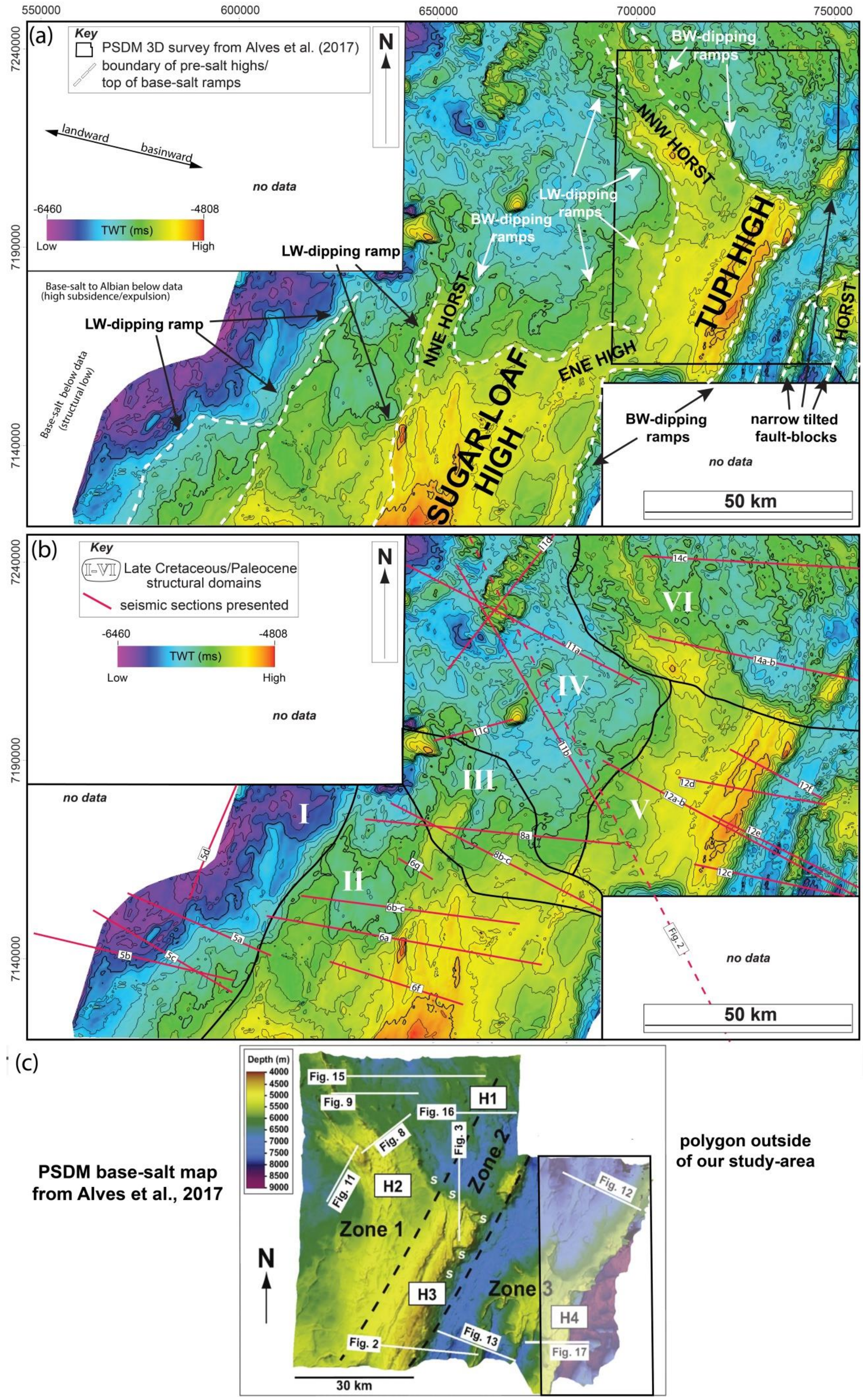
(a)
Key
PSDM 3D survey from Alves et al. (2017)
boundary of pre-salt highs/
top of base-salt ramps
landward
basinward
no data
-6460
-4808
TWT (ms)
Low
High
LW-dipping ramp
Base-salt to Albian below data
(high subsidence/expulsion)
LW-dipping ramp
Base-salt below data
(structural low)
BW-dipping ramps
NNW HORST
LW-dipping ramps
BW-dipping ramps
NNE HORST
TUPI HIGH
HORST
ENE HIGH
SUGAR-LOAF HIGH
BW-dipping ramps
narrow tilted fault-blocks
no data
50 km
(b)
Key
I-VI Late Cretaceous/Paleocene structural domains
seismic sections presented
-6460
-4808
TWT (ms)
Low
High
no data
no data
I
II
III
IV
V
VI
Fig. 2
no data
50 km
(c)
Depth (m)
Fig. 15
Fig. 9
Fig. 16
H1
Fig. 8
Fig. 3
Fig. 11
H2
Zone 1
Zone 2
Zone 3
H3
H4
Fig. 12
Fig. 2
Fig. 13
Fig. 17
30 km
PSDM base-salt map
from Alves et al., 2017
polygon outside
of our study-area

1289

Figure 3

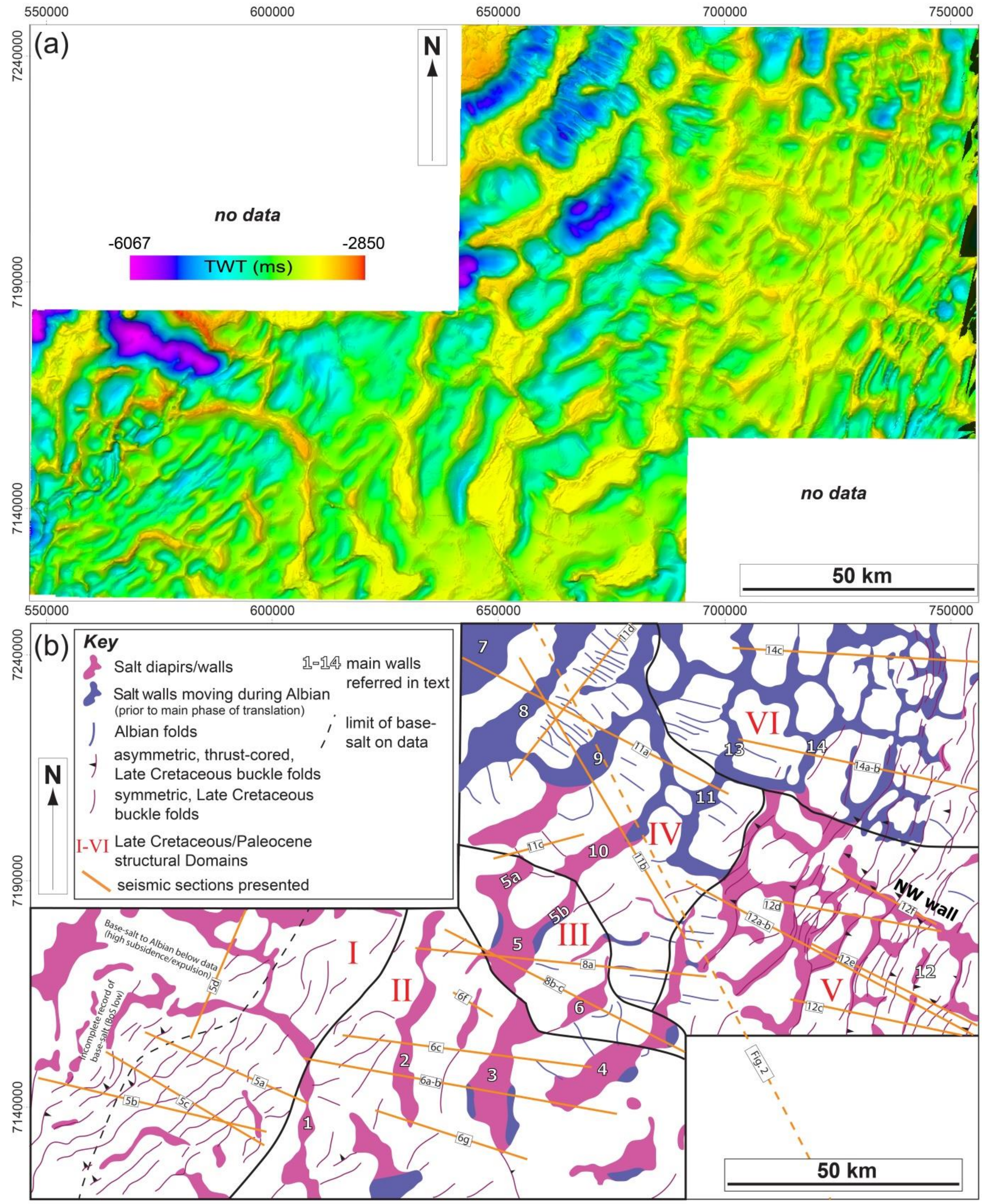

Figure 4

1293
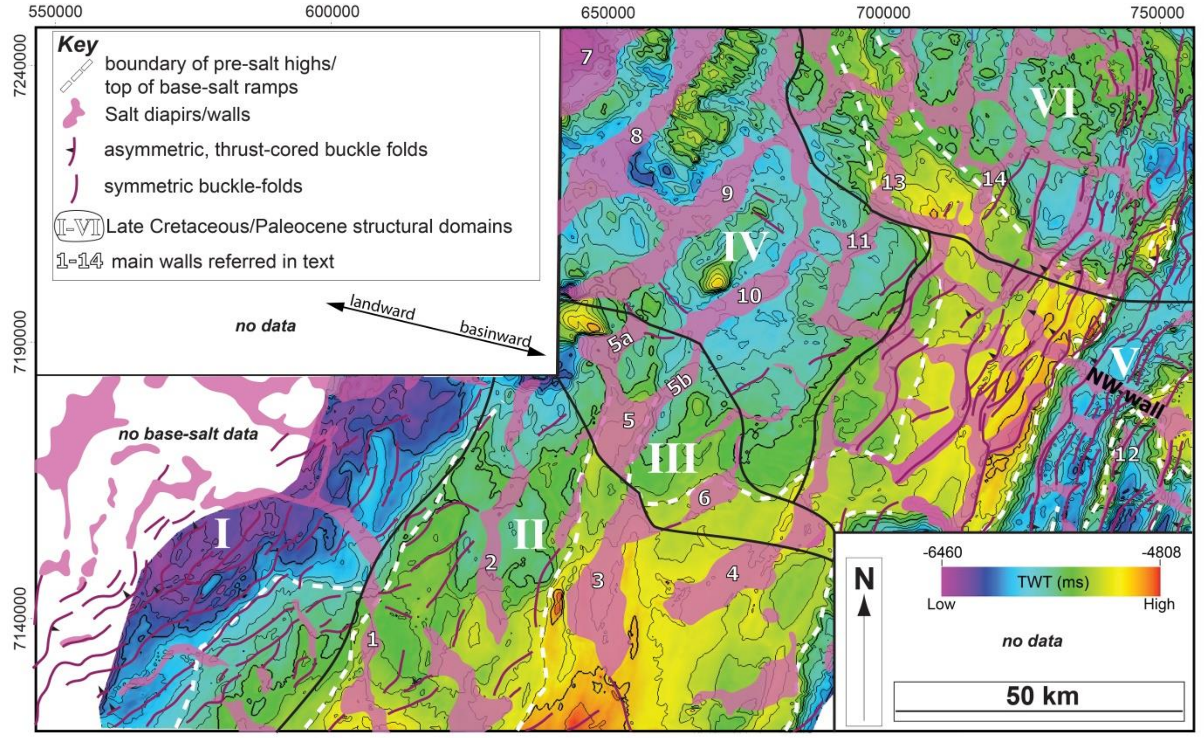

1294 Figure 5

1295

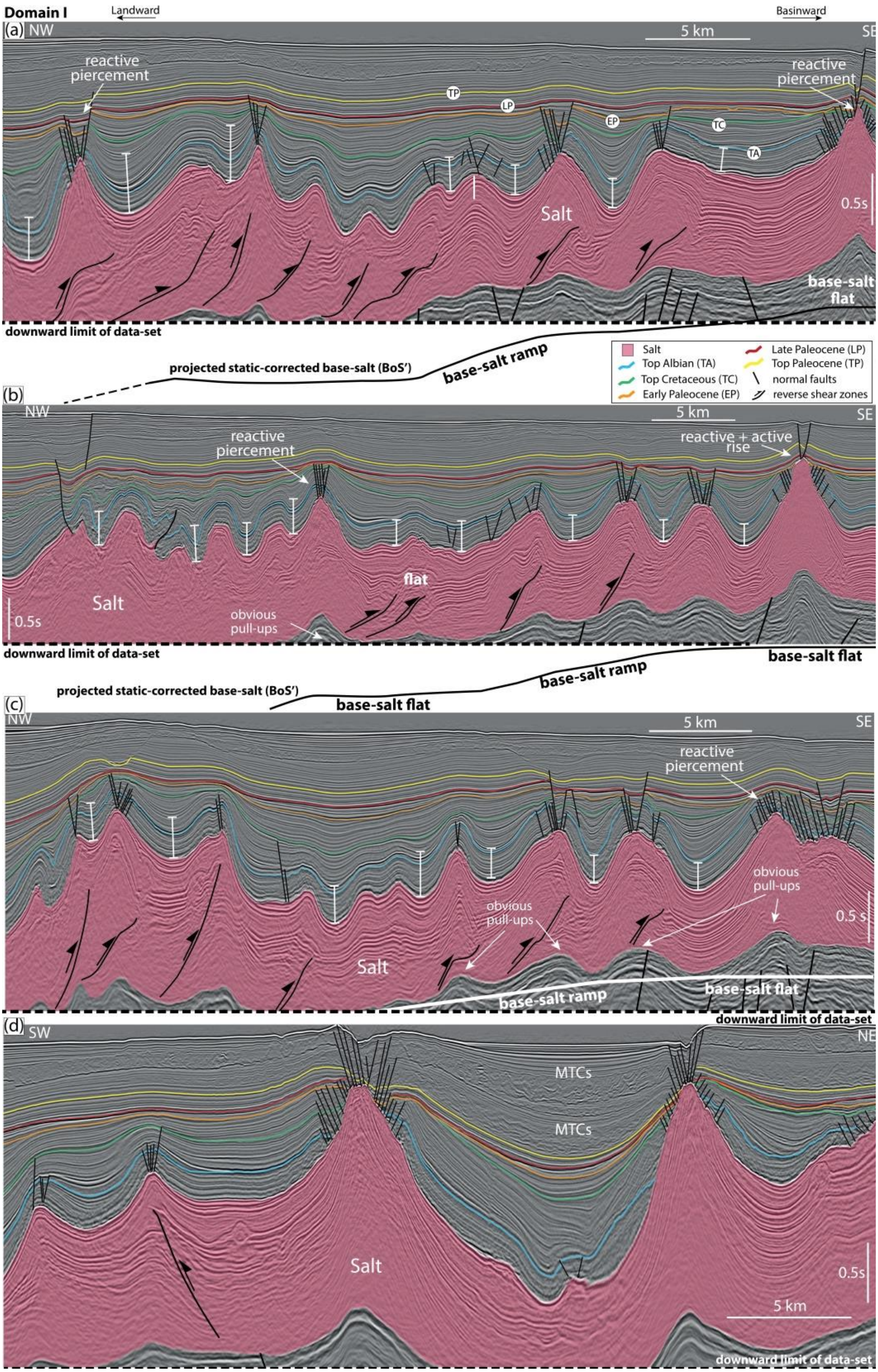

Domain I
Landward
Basinward
(a) NW
SE
5 km
reactive piercement
reactive piercement
TP
LP
EP
TC
TA
Salt
0.5s
base-salt flat
downward limit of data-set
projected static-corrected base-salt (BoS')
base-salt ramp
Salt
Top Albian (TA)
Top Cretaceous (TC)
Early Paleocene (EP)
Late Paleocene (LP)
Top Paleocene (TP)
normal faults
reverse shear zones
(b) NW
SE
5 km
reactive piercement
reactive + active rise
flat
Salt
0.5s
obvious pull-ups
downward limit of data-set
base-salt flat
projected static-corrected base-salt (BoS')
base-salt ramp
base-salt flat
(c) NW
SE
5 km
reactive piercement
obvious pull-ups
obvious pull-ups
0.5 s
Salt
base-salt ramp
base-salt flat
downward limit of data-set
(d) SW
NE
MTCs
MTCs
Salt
0.5s
5 km
downward limit of data-set

1296

Figure 6

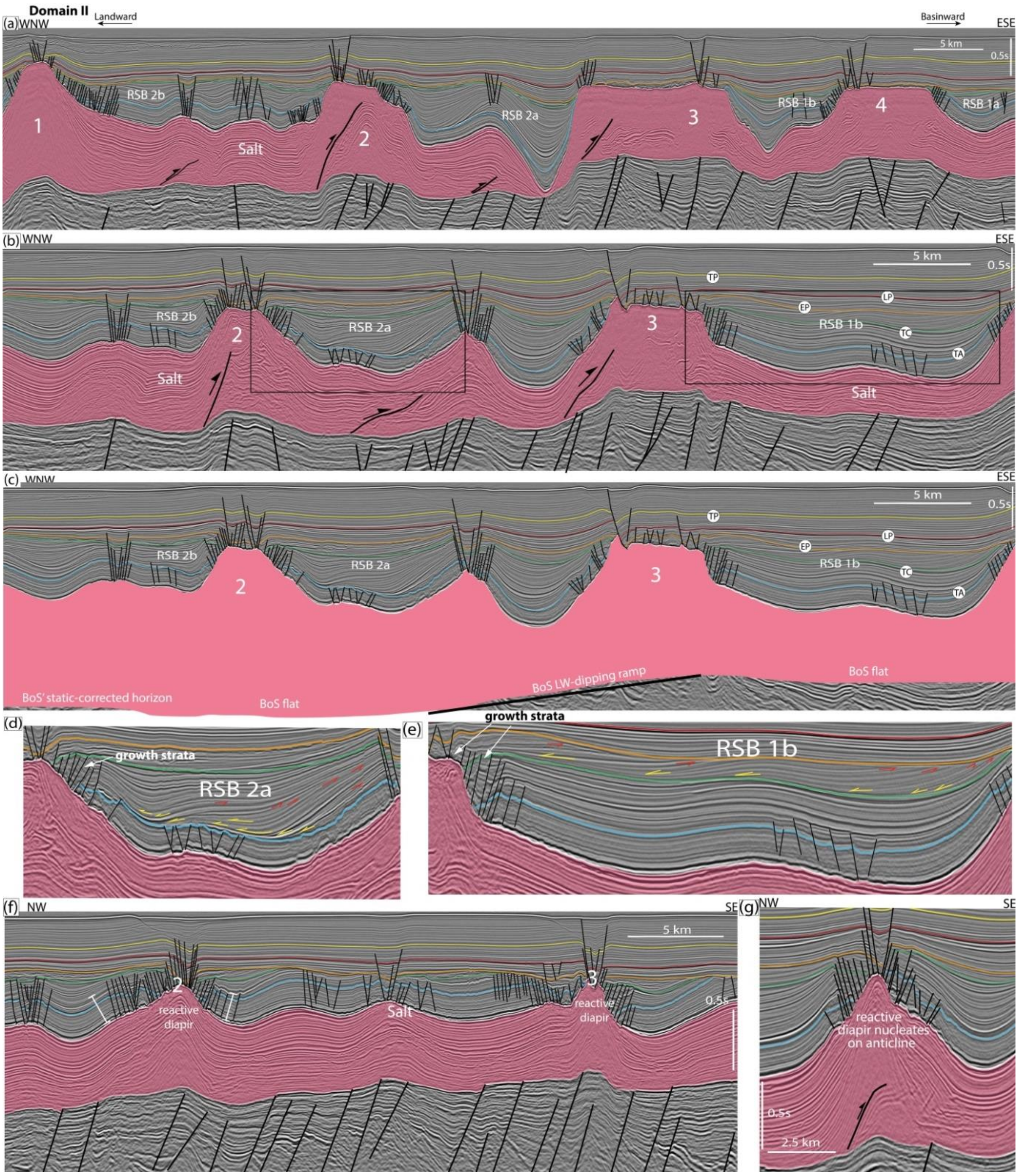

Figure 7

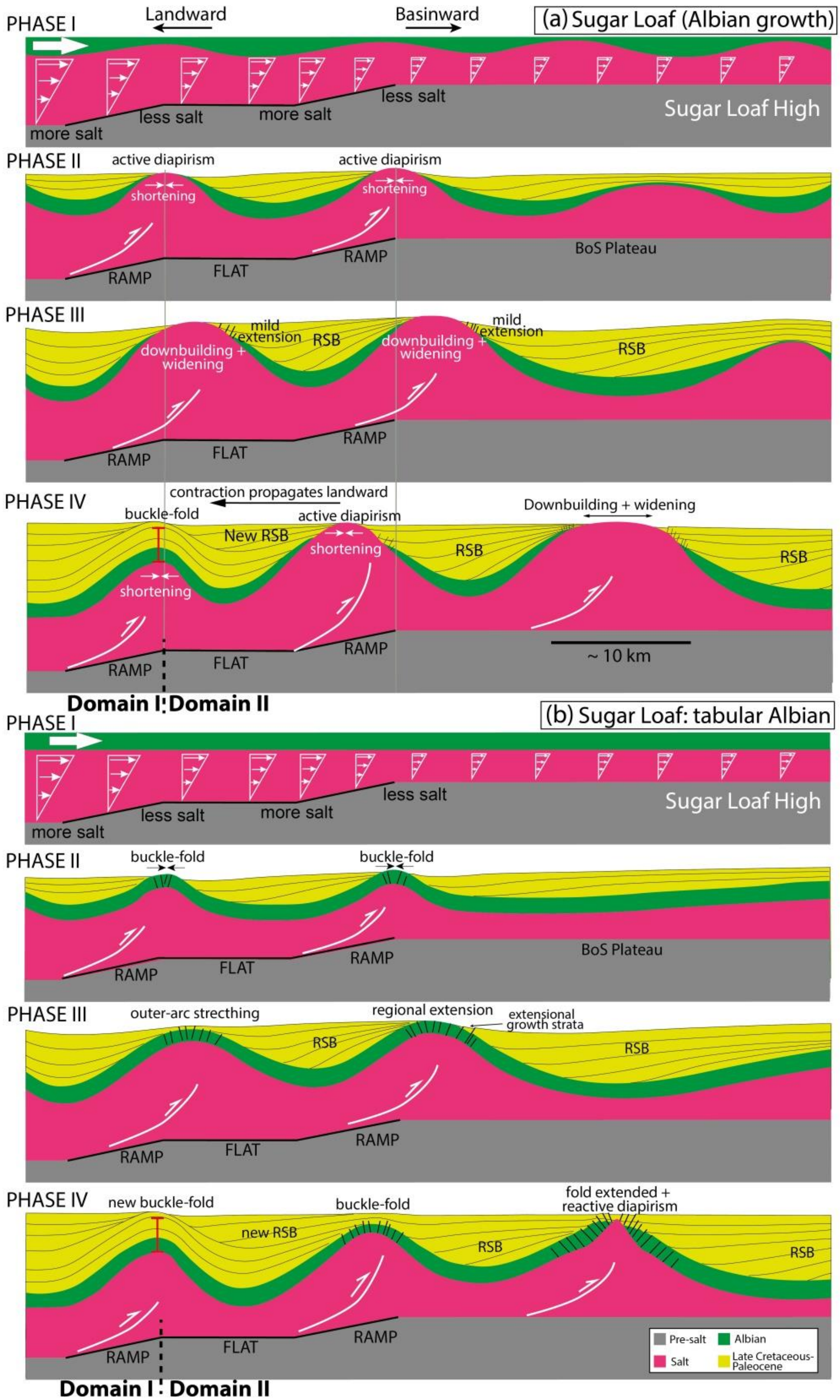
PHASE I
Landward
Basinward
(a) Sugar Loaf (Albian growth)
more salt
less salt
more salt
less salt
Sugar Loaf High
PHASE II
active diapirism
shortening
active diapirism
shortening
RAMP
FLAT
RAMP
BoS Plateau
PHASE III
mild extension
RSB
downbuilding + widening
mild extension
downbuilding + widening
RSB
RAMP
FLAT
RAMP
PHASE IV
contraction propagates landward
buckle-fold
New RSB
active diapirism
shortening
RSB
Downbuilding + widening
RSB
shortening
RAMP
FLAT
RAMP
~ 10 km
Domain I Domain II
(b) Sugar Loaf: tabular Albian
PHASE I
more salt
less salt
more salt
less salt
Sugar Loaf High
PHASE II
buckle-fold
buckle-fold
RAMP
FLAT
RAMP
BoS Plateau
PHASE III
outer-arc strecthing
regional extension
extensional growth strata
RSB
RSB
RAMP
FLAT
RAMP
PHASE IV
new buckle-fold
new RSB
buckle-fold
RSB
fold extended + reactive diapirism
RSB
RAMP
FLAT
RAMP
Pre-salt
Albian
Salt
Late Cretaceous-Paleocene
Domain I Domain II

Figure 8

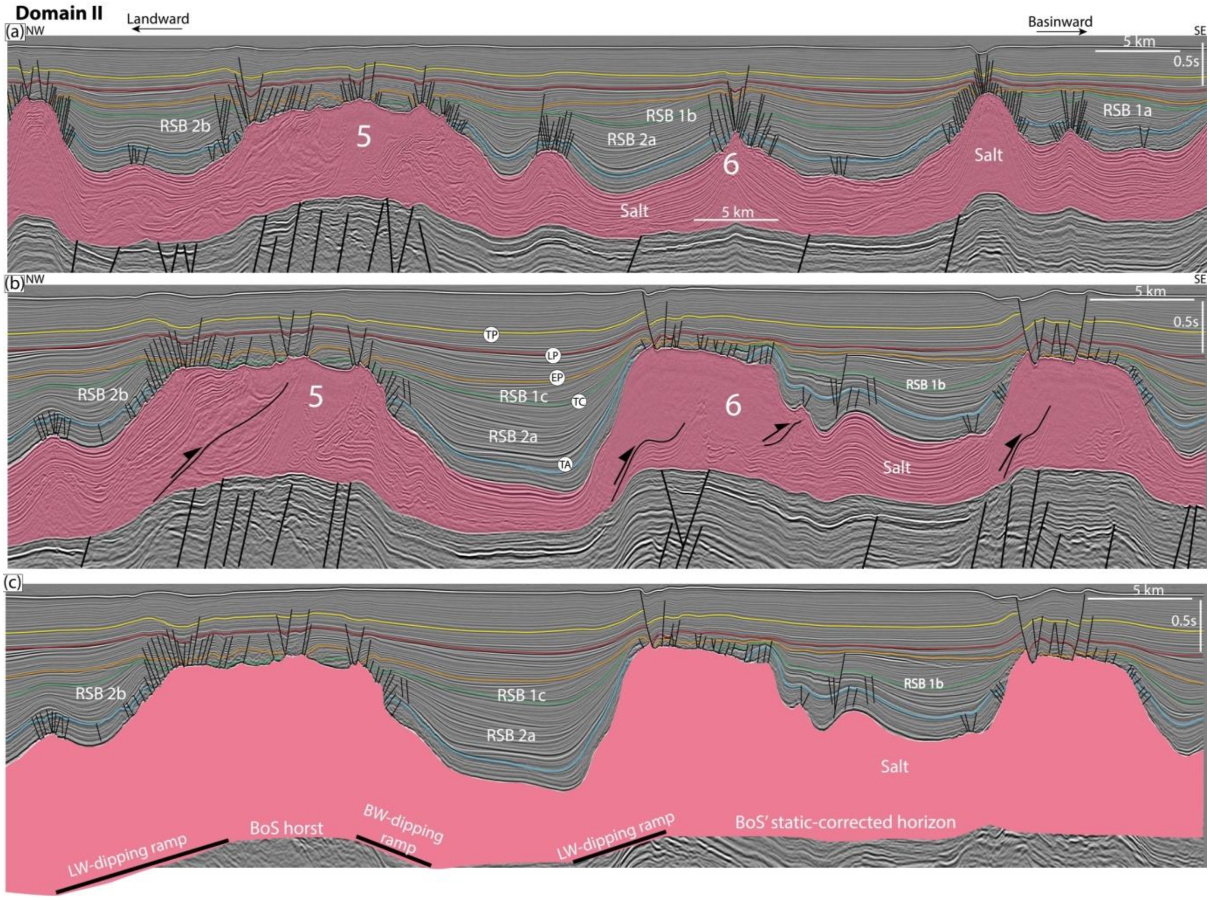

Figure 9

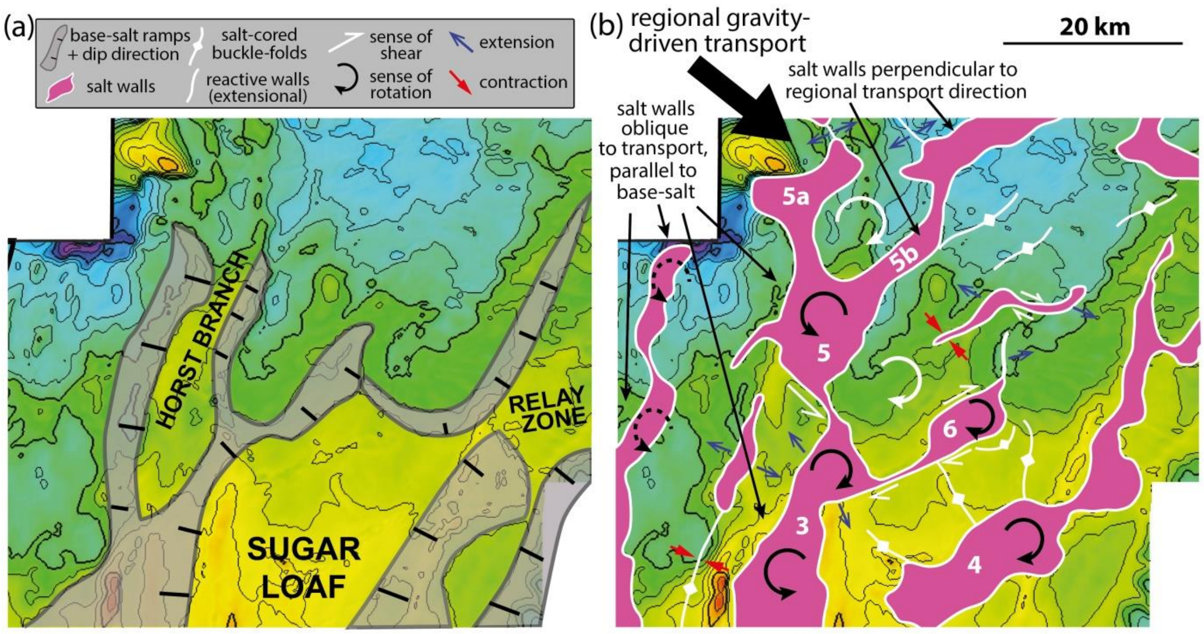

Figure 10

1307
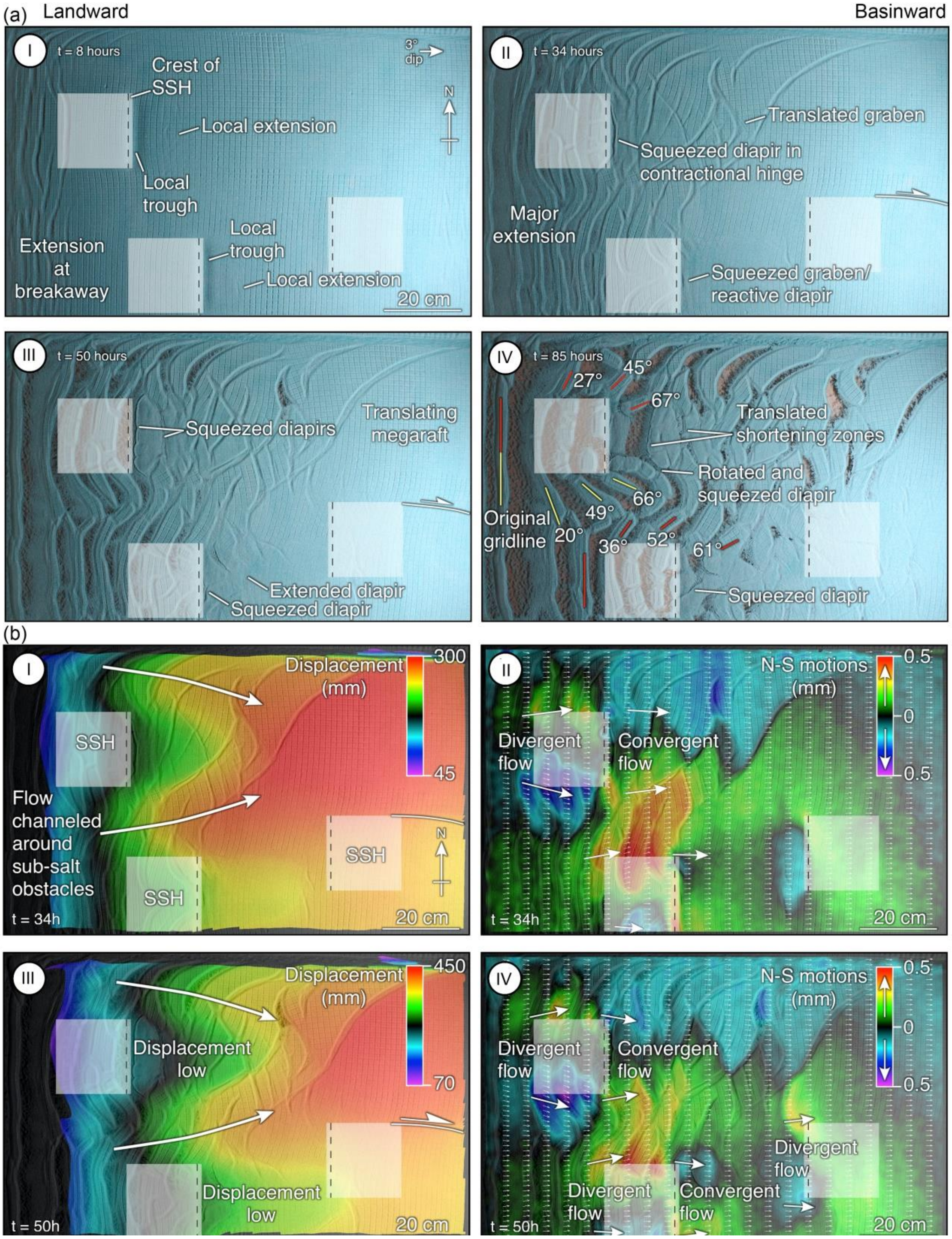

1308 Figure 11

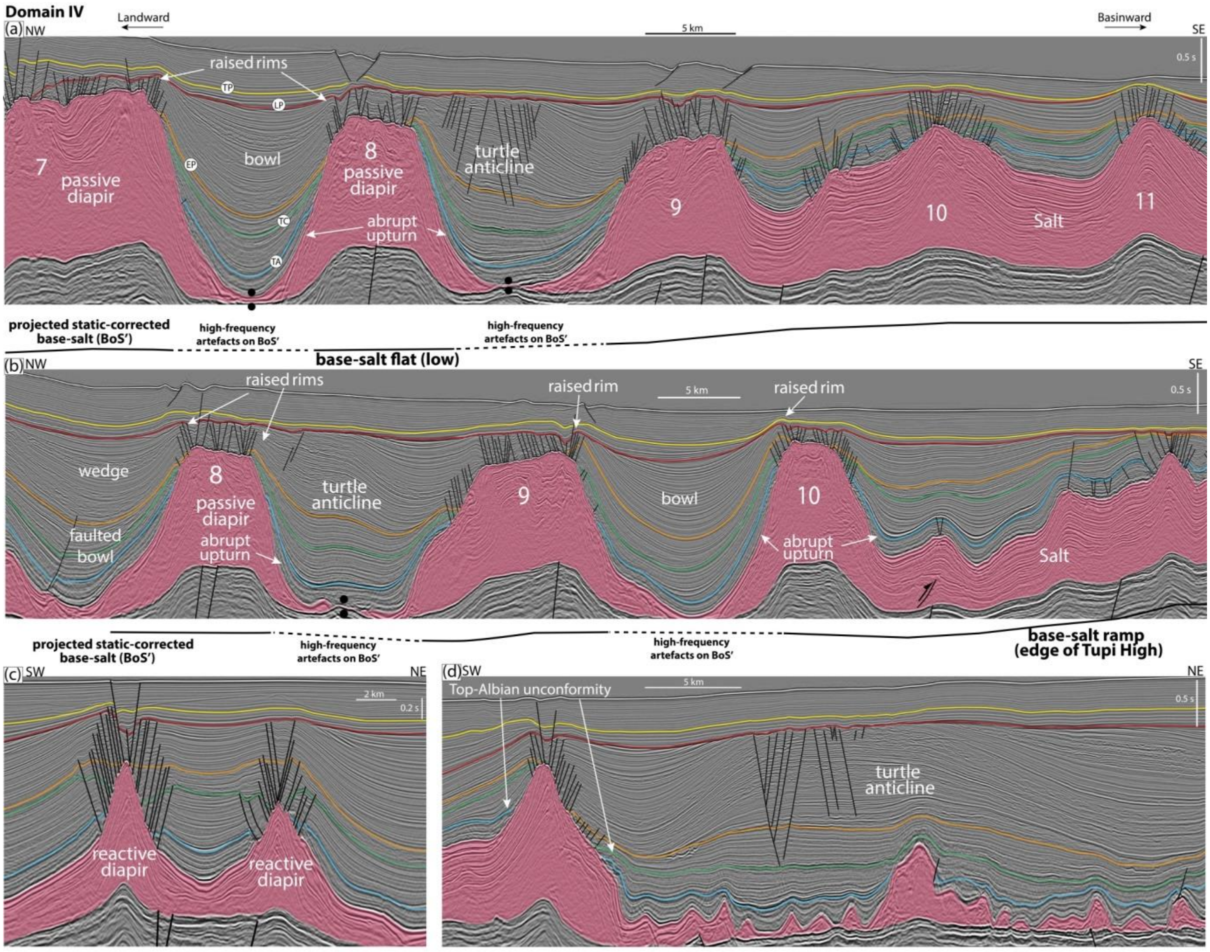
Domain IV
(a) NW
Landward
5 km
Basinward
SE
0.5 s
raised rims
TP
LP
EP
TC
TA
7
passive diapir
bowl
8
passive diapir
turtle anticline
abrupt upturn
9
10
Salt
11
projected static-corrected base-salt (BoS′)
high-frequency artefacts on BoS′
high-frequency artefacts on BoS′
base-salt flat (low)
(b) NW
SE
raised rims
raised rim
5 km
raised rim
0.5 s
wedge
8
passive diapir
turtle anticline
9
bowl
10
faulted bowl
abrupt upturn
abrupt upturn
Salt
projected static-corrected base-salt (BoS′)
high-frequency artefacts on BoS′
high-frequency artefacts on BoS′
base-salt ramp (edge of Tupi High)
(c) SW
NE
2 km
0.2 s
reactive diapir
reactive diapir
(d) SW
Top-Albian unconformity
5 km
NE
0.5 s
turtle anticline

Figure 12

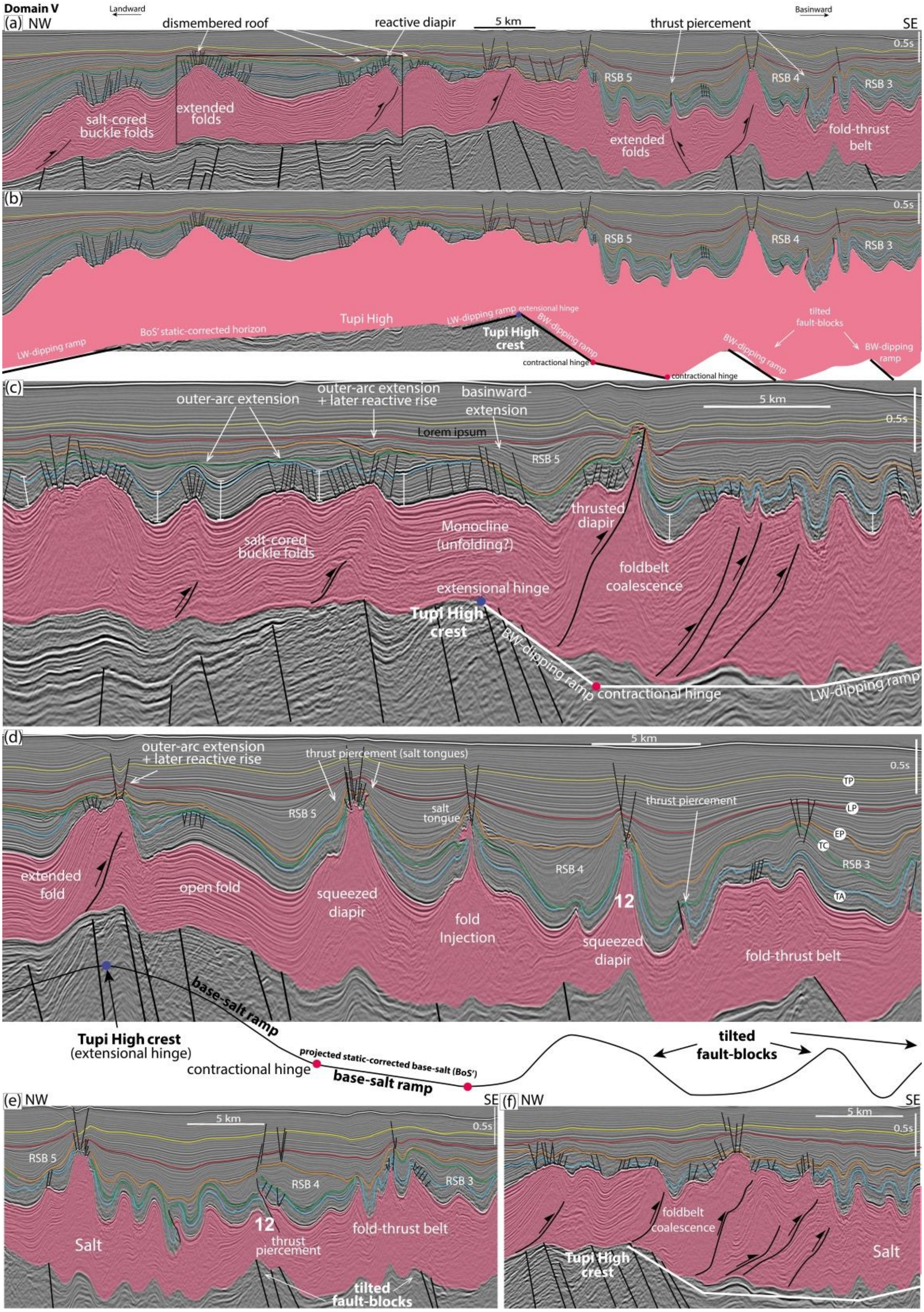
Domain V
(a) NW
Landward
dismembered roof
reactive diapir
5 km
thrust piercement
Basinward
SE
0.5s
RSB 5
RSB 4
RSB 3
salt-cored buckle folds
extended folds
extended folds
fold-thrust belt
(b)
0.5s
RSB 5
RSB 4
RSB 3
Tupi High
LW-dipping ramp
BoS' static-corrected horizon
LW-dipping ramp
extensional hinge
Tupi High crest
BW-dipping ramp
contractional hinge
contractional hinge
BW-dipping ramp
tilted fault-blocks
BW-dipping ramp
(c)
outer-arc extension
outer-arc extension + later reactive rise
basinward-extension
5 km
0.5s
Lorem ipsum
RSB 5
thrusted diapir
Monocline (unfolding?)
salt-cored buckle folds
foldbelt coalescence
extensional hinge
Tupi High crest
BW-dipping ramp
contractional hinge
LW-dipping ramp
(d)
outer-arc extension + later reactive rise
thrust piercement (salt tongues)
5 km
0.5s
RSB 5
salt tongue
thrust piercement
TP
LP
EP
TC
RSB 3
TA
RSB 4
extended fold
open fold
squeezed diapir
fold Injection
12
squeezed diapir
fold-thrust belt
Tupi High crest
(extensional hinge)
base-salt ramp
contractional hinge
projected static-corrected base-salt (BoS')
base-salt ramp
tilted fault-blocks
(e) NW
5 km
SE
0.5s
RSB 5
RSB 4
RSB 3
Salt
12
thrust piercement
fold-thrust belt
tilted fault-blocks
(f) NW
5 km
SE
0.5s
foldbelt coalescence
Tupi High crest
Salt

Figure 13

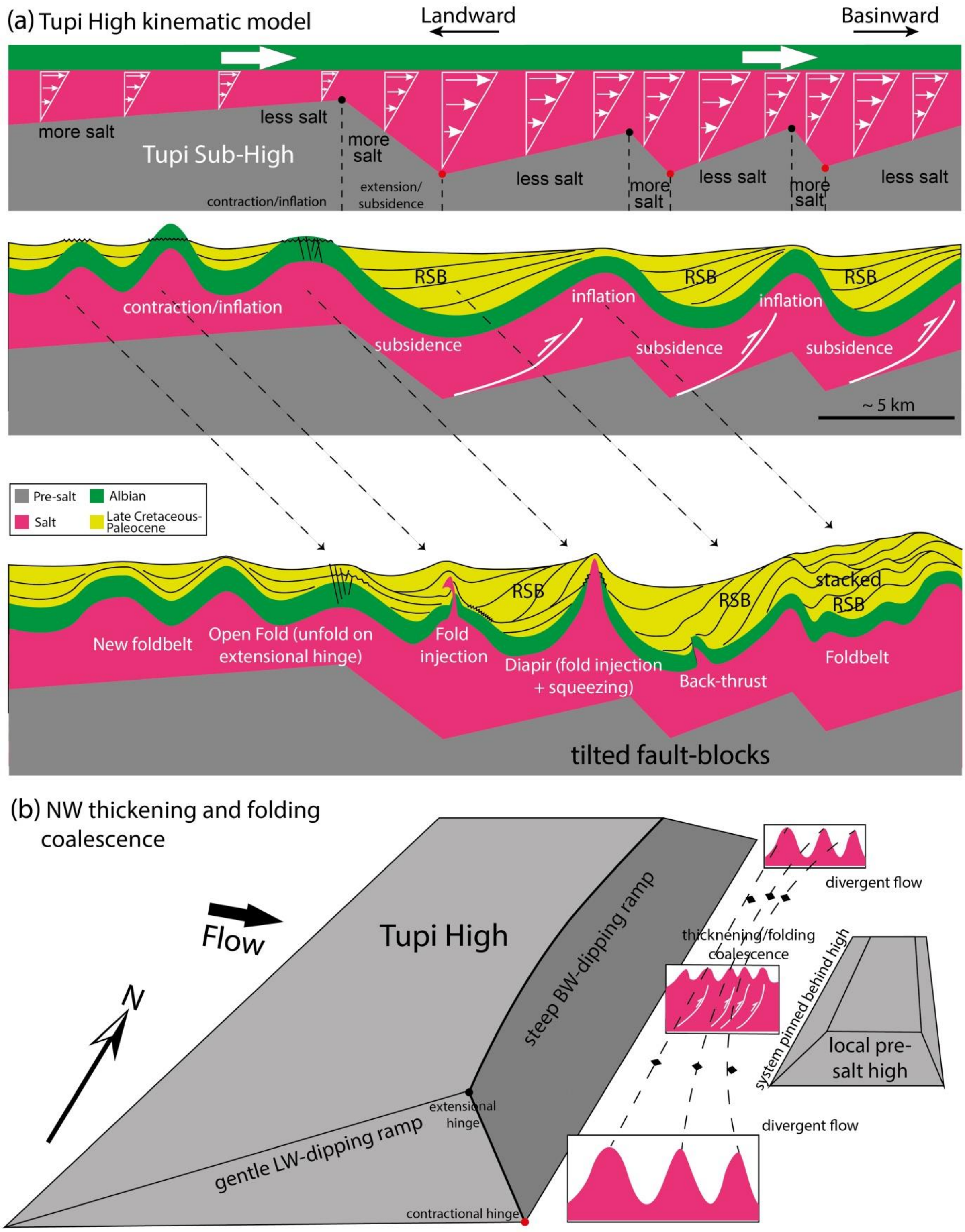

1313

1314 Figure 14

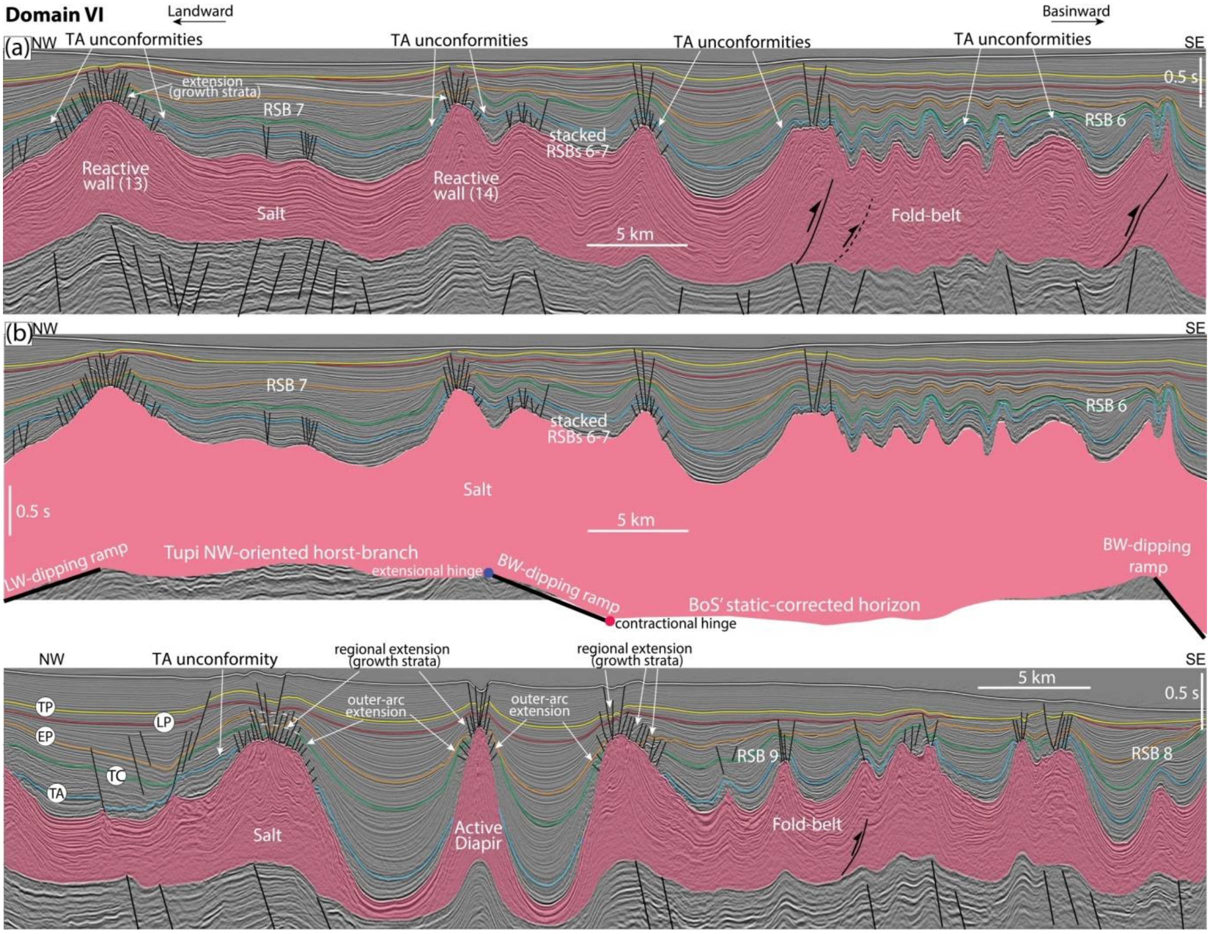
Domain VI
Landward
Basinward
(a)
NW
TA unconformities
TA unconformities
TA unconformities
TA unconformities
SE
0.5 s
extension
(growth strata)
RSB 7
stacked
RSBs 6-7
RSB 6
Reactive
wall (13)
Reactive
wall (14)
Salt
Fold-belt
5 km
(b)
NW
SE
RSB 7
stacked
RSBs 6-7
RSB 6
Salt
0.5 s
5 km
LW-dipping ramp
Tupi NW-oriented horst-branch
extensional hinge
BW-dipping ramp
contractional hinge
BoS' static-corrected horizon
BW-dipping
ramp
NW
TA unconformity
regional extension
(growth strata)
regional extension
(growth strata)
SE
5 km
0.5 s
outer-arc
extension
outer-arc
extension
TP
LP
EP
TC
TA
RSB 9
RSB 8
Salt
Active
Diapir
Fold-belt

Figure 15

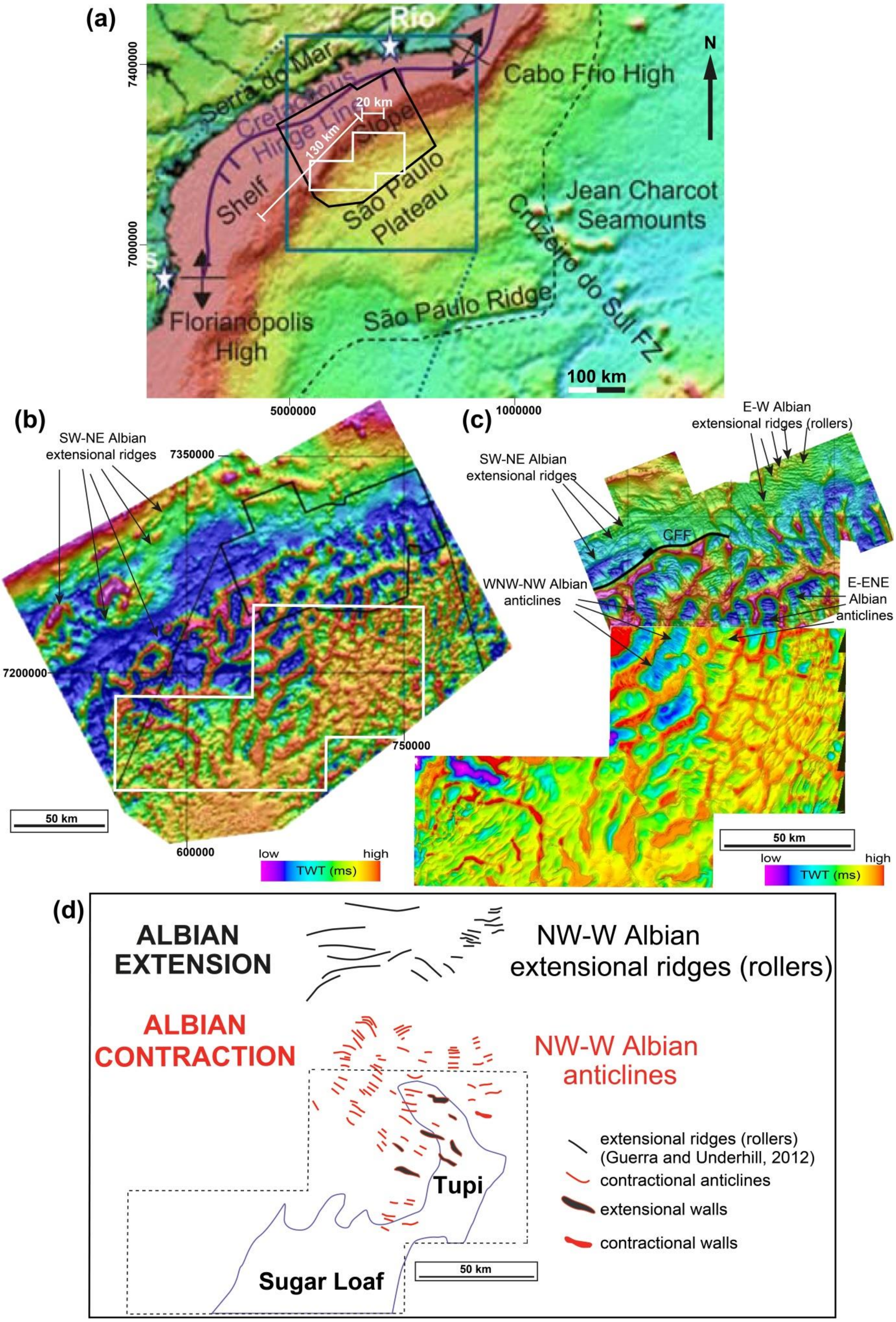

1317
1318 Figure 16

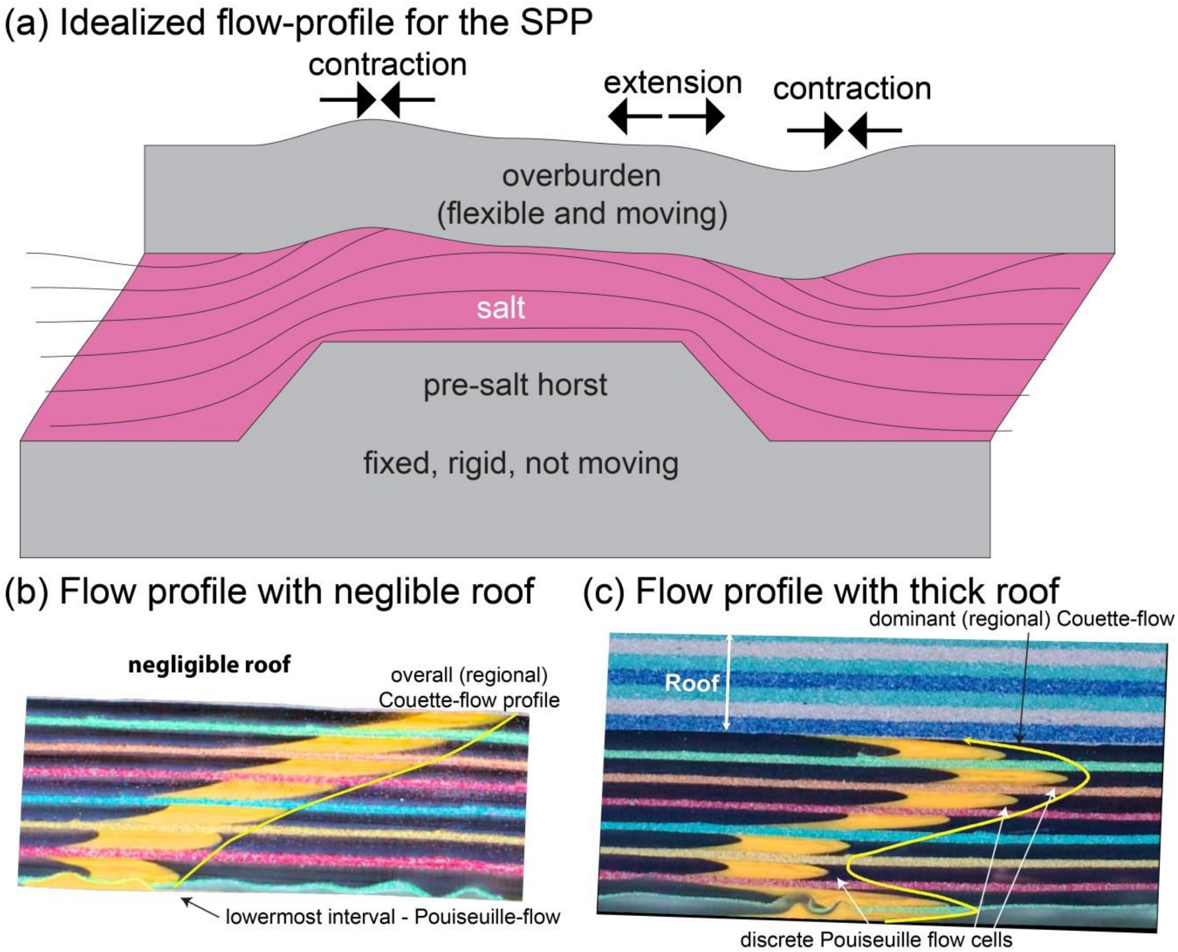

Figure 17

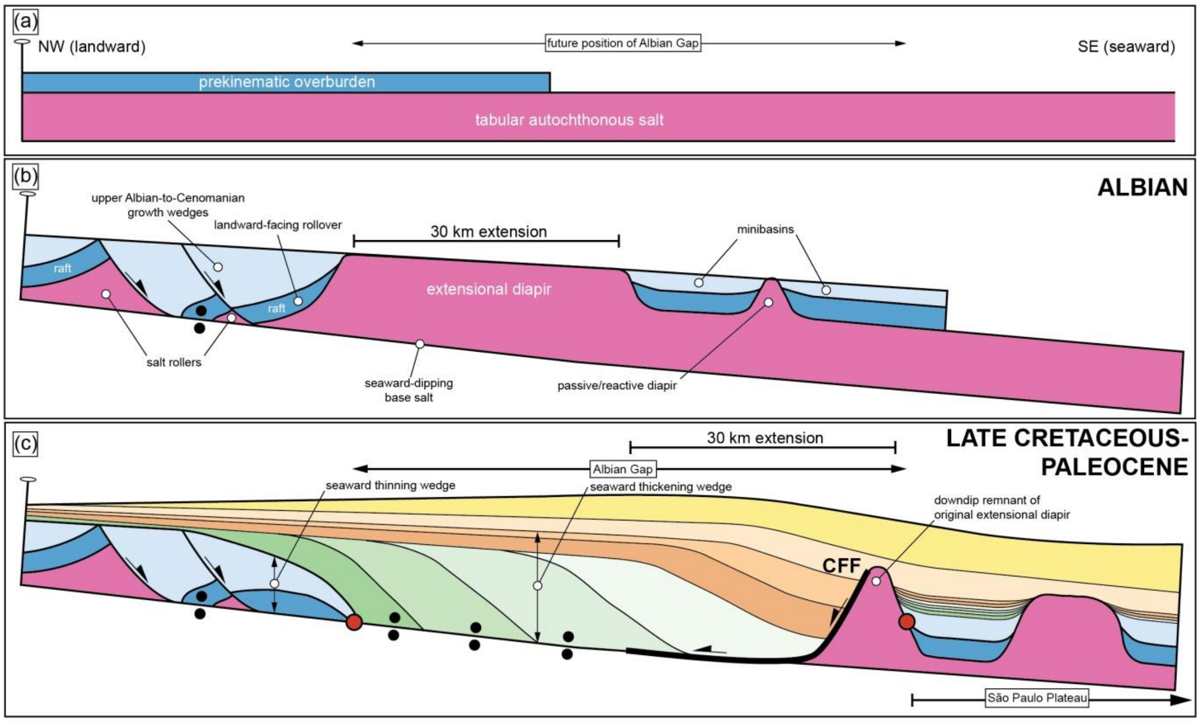

Figure 1

Appendix Figure Table

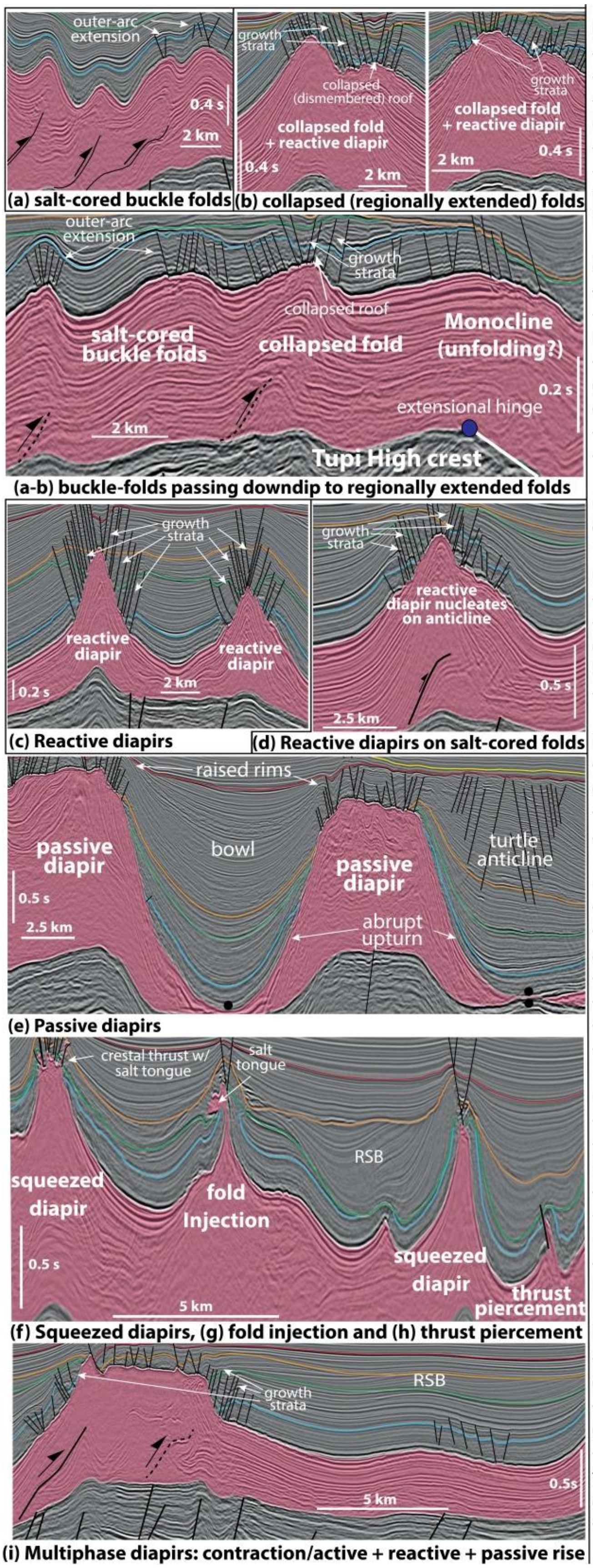

(a) salt-cored buckle folds
- commonly cored by intra-salt reverse shear zones
- broadly tabular roof
- crestal normal faults with no syn-sedimentary growth (hangingwall strata at regional) denote out-arc stretching
- vary from rounded, sinosuidal to box-shaped
- occur above landward-dipping base-salt ramps (Domains I & II) and downdip of basinward-dipping base-salt ramps (contractional hinges, **Domains V** & **VI**)

(b) collapsed (regionally-extended) folds
- similar to (a) but with typically gentler profiles
- normal faults show syn-sedimentary growth (thicker and below-regional hangingwall strata) denote roof collapse
- extension can be asymmetric: dominance of basinward-dipping normal faults and development of monoclinal geometries by unfolding over basinward-dipping ramps
- can lead to diapir piercement **(c-d)**
- occur over base-salt horsts (**Domains II-III** & **V-VI**)

(a-b) buckle-folds passing to collapsed/extended folds downdip near extensional hinge at crest of Tupi High

(c) Reactive diapirs
- triangular profiles with gently-dipping flank strata
- inward-dipping and younging normal faults with syn-extensional growth strata (hangingwall thickening and below regional)
- occur over base-salt flats & horsts (**Domains II-III** & **VI**)

(d) Reactive diapirs nucleating on salt-cored folds
- similar to **(c)** but forming over inflated, rounded salt-cored folds with intra-salt reverse shear zones
- occur over base-salt horsts (**Domains II-III** & **VI**) and near extensional hinges (**Domains V** & **VI**)

(e) Passive diapirs
- tall (c. 4 km) diapirs with thick, welded minibasins
- minibasins are highly symmetric with vertically-aligned axial traces (bowls) or turtle anticlines
- raised bathymetric rims at their flanks
- abrupt and broadly symmetric upturn of flank strata
- Early (Albian) growth and limited lateral deformation
- occur in **Domain IV**, away of large pre-salt structures

(f) Squeezed diapirs (contractional - Domain V)
- narrow (< 2 km wide) diapirs with abrupt flank upturns
- occasionally with crestal thrusts and small salt tongues

(g) Fold-injection (contractional - Domain V)
- narrow (< 1 km) diapirs on the crest of salt-cored folds
- ocasionally developing salt tongues at their crest

(h) thrust-piercement (contractional - Domain V)
- narrow, leaning (typically landward) diapirs forming by thrusting at the crest of salt-cored folds

(i) Multiphase diapirs
- complex intra-salt deformation and reverse shearing denoting **early contraction or active rise**
- inward-dipping and younging normal faults with syn-extensional growth strata denote **extension/reactive rise**
- their large width (> 10 km) suggests they reached the sea-floor after extension, pointing to late passive diapirism and/or cryptic extension
- Occur over the large base-salt plateau (**Domains II-III**)